Importin α Accumulates in Micronuclei and Associates with Genomic Instability in Human Cancer Cells

Yoichi Miyamoto[1,2*], Reo Kisanuki[3], Rieko Oshima[1,2], Shige H. Yoshimura[4,5], Mutsumi Yokota[6], Kazumitsu Maehara[7], Chiaki Hata[8], Taro Tachibana[8,9], Masato Koike[6], Yasuyuki Ohkawa[7], Toyomasa Katagiri[2], Yoshihiro Yoneda[10], Masahiro Oka[1,11], and Hisato Saitoh[3,12*]

[1]Laboratory of Nuclear Transport Dynamics, and [2]Laboratory of Biofunctional Molecular Medicine, Center for Drug Design Research, National Institutes of Biomedical Innovation, Health and Nutrition (NIBIOHN), Osaka, Japan.

[3]Department of Biological Science, Graduate School of Science and Technology, Kumamoto University, Kumamoto, Japan.

[4]Graduate School of Biostudies, Kyoto University, Kyoto, Japan

[5]Center for Living Systems Information Science (CeLiSIS), Kyoto University, Kyoto, Japan

[6]Department of Cell Biology and Neuroscience, Juntendo University Graduate School of Medicine, Tokyo, Japan

[7]Division of Transcriptomics Medical Institute of Bioregulation, Kyushu University, Fukuoka, Japan.

[8]Cell Engineering Corporation, Osaka, Japan.

[9]Department of Bioengineering, Graduate School of Engineering, Osaka Metropolitan University, Osaka, Japan.

[10]The Research Foundation for Microbial Diseases of Osaka University, Suita, Osaka, Japan

[11]Department of Regulation of Infectious Cancer, Research Institute of Microbial Diseases (RIMD), Osaka University, Suita, Osaka, Japan

[12]Faculty of Advanced Science and Technology (FAST), Kumamoto University, Kumamoto, Japan.

[*]Correspondence:

Y. Miyamoto, E-mail: ymiyamoto@nibiohn.go.jp; *Laboratory of Biofunctional Molecular Medicine, Center for Drug Design Research, National Institutes of Biomedical Innovation, Health and Nutrition (NIBIOHN), 7-6-8 Saito-Asagi, Ibaraki-shi, Osaka 567-0085, Japan*

H. Saitoh, E-mail: hisa@kumamoto-u.ac.jp; *Faculty of Advanced Science and Technology (FAST), Kumamoto University, 2-39-1 Kurokami, Chuo-ku, Kumamoto 860-8555, Japan*

Running title: Importin α in micronuclei.

Keywords: Cancer development, Chromatin, DNA damage, Genome instability, Micronucleus, Nuclear transport

Summary statement: Accumulation of importin α in micronuclei, followed by alteration of their microenvironment, suggests the non-canonical function of importin α in genomic instability and cancer development.

ABSTRACT

Micronuclei (MN), are membrane-enclosed structures that contain DNA or chromatin, are biomarkers of genome instability. Here, we report that importin α, a key nuclear transport factor, is highly concentrated in the MN of cultured human cancer cells. Notably, it is not uniformly distributed, but is localized to approximately 40% of the MN. This selective localization is characterized by an uncorrelated distribution relative to importin β1, CAS/CSE1L, and Ran, suggesting that the nucleocytoplasmic recycling of importin α is uncontrolled in the MN. We found that the subset of importin α-positive MN exhibits collapsed nuclear envelopes and compromised barrier functions. In addition to an association with euchromatin regions, we identified that chromatin-regulating molecules potentially interact with importin α and noted a significant reduction in the mobility of importin α within MN. These observations indicate that a unique state is established in importin α-enriched structures. Importantly, our findings reveal a mutually exclusive relationship between the accumulation of importin α and RAD51, a protein involved in homologous recombination repair, in MN. These results suggest that importin α is an unrecognized molecular marker for assessing genomic stability in human cancer cells.

58 **INTRODUCTION**

59 Micronuclei (MN) are cytoplasmic structures embedded within the nuclear envelopes but spatially
60 separated from primary nuclei (PN). MN arise from lagging chromosomes or chromosome
61 fragments produced by mitotic errors or DNA damage after genotoxic stress (Hintzsche *et al*, 2017;
62 Kwon *et al*, 2020). Thus, the MN are biomarkers of genome instability, including forms such as
63 chromosome rearrangements, mutagenesis, and chromothripsis (Krupina *et al*, 2021; Kwon *et al.*,
64 2020; Zhang *et al*, 2015). In particular, the study of chromothripsis in many aggressive types of
65 cancer has been rapidly expanding and advancing; research suggests that MN actively participates
66 in chromothripsis during cancer development, progression, and genome evolution (Forment *et al*,
67 2012; Ly & Cleveland, 2017; Storchová & Kloosterman, 2016). Moreover, the exposure of
68 DNA/chromatin fibers within MN to cytoplasmic components can serve as a potent molecular
69 pattern signal by activating sterile inflammatory responses, which are associated with many
70 chronic age-associated conditions (Miller *et al*, 2021).

71 Signal-dependent protein transport occurs through nuclear pore complexes (NPCs)
72 embedded in the nuclear envelope (Fernandez-Martinez & Rout, 2021; Hampoelz *et al*, 2019;
73 Knockenhauer & Schwartz, 2016). Importin α is a classical nuclear localization signal (cNLS)
74 receptor that acts as an adaptor molecule between the cNLS-bearing cargo and their carrier
75 molecule, importin β1 (Goldfarb *et al*, 2004). The cNLS–importin α–importin β1 trimeric complex
76 migrates into the nucleus via mediation by the Ras-like small GTPase, Ran, and dissociates upon
77 the binding of importin β1 and RanGTP (Christie *et al*, 2016; Wente & Rout, 2010). Importin α is
78 exported to the cytoplasm by cellular apoptosis susceptibility gene product (CAS), also known as
79 chromosome segregation 1-like protein [CSE1L; (Behrens *et al*, 2003; Stewart, 2007)]. Human
80 express seven importin α subtypes, including importin α1 (KPNA2), importin α3 (KPNA4),
81 importin α4 (KPNA3), importin α5 (KPNA1), importin α6 (KPNA5), importin α7 (KPNA6), and

82 importin α8 (KPNA7), which exhibit distinct cNLS-binding specificities and selective expression
83 in various tissues (Goldfarb *et al.*, 2004; Miyamoto *et al*, 2012; Pumroy & Cingolani, 2015).
84 Importin α1/KPNA2 has been well investigated, and high expression levels of this protein are
85 associated with poor prognoses of various cancers (Han & Wang, 2020; Sun *et al*, 2021; Wang *et*
86 *al*, 2012). Notably, strong nuclear staining of importin α1 in breast cancer cells using
87 immunohistochemical analysis is significantly associated with a higher tumor stage (Alshareeda *et*
88 *al*, 2015; Dahl *et al*, 2006; Dankof *et al*, 2007).

89 In addition to nucleocytoplasmic transport regulation, importin α plays non-transport roles
90 in spindle assembly regulation, lamin polymerization, nuclear envelope formation, protein
91 degradation, stress response, gene expression, cell surface response, and mRNA metabolism,
92 which emphasizes its multi-functionality (Miyamoto *et al*, 2016; Oka & Yoneda, 2018). Importin
93 α accumulates in the nucleus under exceptional conditions, e.g., stress responses, in which it binds
94 to a DNase-sensitive nuclear component, indicating its potential to associate with DNA/chromatin
95 (Furuta *et al*, 2004; Kodiha *et al*, 2008; Miyamoto *et al*, 2004). We have demonstrated that nuclear-
96 localized importin α associates with chromatin and regulates its gene expression (Yasuda *et al*,
97 2012). A recent report suggests that the importin β binding (IBB) domain enables the binding of
98 importin α to DNA (Jibiki *et al*, 2021). These findings indicate that the nuclear-localized importin
99 α can function as a regulator for nuclear homeostasis through its intrinsic capacity for
100 DNA/chromatin binding.

101 In this study, we investigated the dynamics and functions of importin α in several human
102 cancer cell lines. We discovered that a considerable concentration of importin α in MN. Our
103 findings indicate that the micronuclear localization of importin α does not fully align with its
104 conventional role and dynamics as a nuclear transport factor. We characterized several interacting
105 chromatin proteins linked to slow mobility of importin α1 in MN. This investigation revealed not

106 only a new molecular marker of MN but also elucidated MN structure and quality in cancerous

107 cells.

RESULTS

Visualization of importin α accumulation in MN

Importin α is highly expressed in various cancer cells; there is a potential association between its high expression levels and the tumor stages and patient survival outcome (Christiansen & Dyrskjot, 2013; Han & Wang, 2020). We validated the enhanced expression of importin α subtypes in breast cancer cell lines (MCF7, MDA-MB-231, and SK-BR-3), along with a control non-transformed human mammary cell line (MCF10A). Western blot assays revealed that importin α, particularly importin α1 (KPNA2), was expressed at higher levels in the cancer cell lines than in the control (Fig. 1A). Indirect immunofluorescence (IF) analysis for identifying the subcellular localization of importin α1 in MCF7 and HeLa cells revealed that the cytoplasm of those cell lines emitted quite strong signals, which were found to originate from MN (MCF7 cells in Fig. 1B, and HeLa cells in Fig. 1C, yellow arrowhead). The MN fluorescence intensity was considerably higher than that of PN or the cytoplasm, to the extent that the latter was almost invisible when normalized against the former (Fig. 1D). We also found that other importin α subtypes—importin α3 (KPNA4), importin α4 (KPNA3), and importin α5 (KPNA1)—were present in MN (Fig. S1A). Furthermore, similar MN subsets contained different subtypes such as importin α3 or importin α5 along with importin α1 (Fig. S1B).

Since MN are known to arise from lagging chromosomes during anaphase, a process associated with chromosome instability, which is a hallmark of cancer cells, we treated cells with an MPS1 inhibitor, reversine, which efficiently induces chromosome mis-segregation and MN formation at [Fig. S2A, and S2B (Agustinus *et al*, 2023; D'Alise *et al*, 2008; Santaguida *et al*, 2010)]. After 20 h treatment of HeLa cells with 400 nM reversine (Fig. S2C), MN were observed in approximately 30 % of the cells (Fig. S2D). We categorized the signal patterns of MN into three groups, based on the IF analyses using the anti-importin α1 antibody: high (yellow

132 arrowhead), low (white arrowhead), or no intensity (white arrow) (Fig. S2E). Among the MN
133 observed in HeLa cells, approximately 30% exhibited high intensity and 10% exhibited low
134 intensity, indicating that up to 40% of the MN showed importin α1 accumulation under both
135 standard culture conditions and the reversine treatment (Fig. S2F).

136 We then examined MN localization of the overexpressed importin α1 fused with enhanced
137 green fluorescence protein (EGFP) or monomeric red fluorescence protein (mRFP) in reversine
138 treated HeLa cells (Fig. 1E). Overexpressed importin α predominantly localizes in PN (Miyamoto
139 *et al*, 2020). Consistent with this finding, more than 60% of the cells expressed EGFP–importin
140 α1 showed PN localization (Fig. 1F). In contrast, similar to the results for endogenous importin
141 α1, approximately 30% of the cells with EGFP–importin α1 displayed signals from some, but not
142 all, MN, whereas both MN and PN localizations were observed in fewer than 3% of the cells (Fig.
143 1E, and 1F). Moreover, mRFP–importin α1 colocalized with EGFP–importin α subtypes, α3, α4,
144 and α5, in the same MN (Fig. S1C), indicating that the accumulation of importin α family
145 members in the MN is a common feature.

146

147 **MN localization of importin α1 is uncharacterized in the context of the conventional nuclear**
148 **transport machinery.**

149 To determine whether the nuclear transport factors known to influence the subcellular localization
150 of importin α coordinate its localization in the importin α1-positive MN, we conducted an indirect
151 IF analysis for importin β1, CAS/CSE1L, and Ran in reversine-treated HeLa cells. Importin β1
152 was predominantly observed in the cytoplasm and at the rim of PN, as well as in MN. However,
153 most importin β1 signals represented the rim of MN, with minimal overlap of importin α1 signals
154 from inside MN (Fig. 2A). Notably, less than 17% of the MN showed importin β1 localization,
155 which was considerably lower than that of importin α1 (Fig. 2B, and 2C). In contrast, CAS/CSE1L

156 and Ran signals were detected from most MN in HeLa cells, with localization rates of up to 88%
157 or 91%, respectively (Fig. 2A-C). These localization patterns suggest that the selective
158 localization of importin α1 in MN is unlikely to results solely from defects in the nuclear export
159 machinery based on the CAS/CSE1L and Ran gradient.

160 We then investigated whether the MN localization of importin α1 is related to the
161 transport of cNLS substrates. HeLa cells expressing mCherry–SV40TNLS contained endogenous
162 importin α1 with a relatively high probability in cNLS-positive MN (Cell #1 yellow arrowhead
163 in Fig. 2D, and 2E). However, cNLS-signals were also detected from importin α1-negative MN
164 (Cell#2, white arrow in Fig. 2D, and 2E), indicating that selective MN localization of importin α1
165 is not necessarily linked to the transport of cNLS substrates into MN.

166 To confirm that the MN localization of importin α1 does not occur due to the interaction
167 with importin β1, CAS/CSE1L and the cNLS-substrates, we tested several importin α1 mutants,
168 including those with the IBB domain deleted (ΔIBB), deficient in cNLS binding (ED), or mutated
169 at the CAS/CSE1L binding domain (C-mut) to express an EGFP fused protein (Fig. S3A). Cells
170 in which overexpressed EGFP–importin α1 localized only in PN were excluded from the analysis
171 (see Fig. 1E, top panels). All the tested mutants were clearly observed in MN (Fig. S3B, yellow
172 arrowheads). In addition, different patterns of PN localization were identified. In contrast to wild-
173 type importin α1, which appeared to be quite clear and localized exclusively in MN, C-mut
174 localized in both of MN and PN (Fig. S3B-3D). The ΔIBB mutant was also observed in PN but
175 to a lesser extent than C-mut. These findings suggest that the subcellular dynamics of importin
176 α1 in PN and MN are quite different; MN localization of importin α1 is regulated by mechanisms
177 distinct from those governing PN localization, which is typically associated with canonical
178 nucleocytoplasmic recycling processes.

179 Taken together, our data suggest that the MN localization of importin α does not entirely

180 conform to its traditional role as a nuclear transport factor.

181

182 **Nuclear envelopes are partially collapsed in the importin α1-enriched MN**

183 Given that MN formation is often linked to nuclear envelope defects that can perturb nuclear
184 trafficking (Guo *et al*, 2020; Hatch *et al*, 2013; Maciejowski & Hatch, 2020), we examined the
185 nuclear envelope of the importin α1-enriched MN using antibodies against lamins B1 and A/C.
186 Indirect IF analysis revealed that neither lamin clearly correlated with the selective MN
187 localization of importin α1 (Fig. 3A, and 3B: Cell#1). Instead, importin α1 tended to concentrate
188 in MN regions deficient in lamins (Fig. 3A, and 3B: Cell#2, see the graphs of the fluorescence
189 intensity in the X-Y lines). Therefore, nuclear envelope defects were confirmed by using the
190 mAb414 antibody, which recognizes nucleoporins (Fig. S4A and S4B). However, this antibody
191 could not be further used in this context due to cross-reactivity with highly concentrated importin
192 α1 in MN (Fig. S4). To additionally scrutinize nuclear envelope collapse in importin α1-positive
193 MN, we performed correlative light and electron microscopy (CLEM) on HeLa cells expressing
194 EGFP–importin α1. Transmission electron microscopy (TEM) images revealed portions of the
195 nuclear envelope with marked weakening (indicated by white arrowheads in Fig. 3C).

196 We then employed an EGFP fused nuclear export signal (NES) to assess nuclear
197 envelope in importin α1-positive MN. In HeLa cells expressing EGFP–NES, EGFP signals were
198 excluded from the importin α1-negative MN (Fig. 3D, white arrows), whereas they originated
199 from importin α1-positive MN (Fig. 3D, yellow arrowheads). Statistical analysis revealed that the
200 fluorescence intensity of the EGFP–NES signal was remarkably higher for importin α1-positive
201 MN (Fig. 3E. and S4F), indicating that their nuclear envelopes had partially collapsed. These
202 results indicated that nuclear envelopes were partially disrupted in a subset of importin α1-
203 positive MN.

204

205 **Epigenetic chromatin status and importin α distribution in MN**

206 Based on our prior findings that importin α can associate with DNase-sensitive chromatin (Yasuda
207 *et al.*, 2012), we assessed the relationship between importin α1 and DNA/chromatin status in MN
208 by examining well-characterized histone H3 modifications. We used tri-methylations at lysine 4
209 and 9 of histone H3 (H3K4me3 and H3K9me3) as markers of euchromatin and heterochromatin
210 regions, respectively. IF analysis showed that importin α1 signals positively correlated with
211 H3K4me3 signals, and negatively correlated with H3K9me3 signals for MDA-MB-231 cells (Fig.
212 4A, and 4B), MCF7 cells (Fig. S5A, and S5B) and HeLa cells (Fig. S5C, and S5D). Notably,
213 regions with lower intensity of importin α1 signals were often located at the peripheral area of the
214 MN near the nuclear envelope, where DNA/chromatin fibers were generally condensed due to the
215 spatial/structural constraints imposed by the nuclear envelope.

216 To explore the chromatin-binding activity of importin α1, we conducted chromatin
217 immunoprecipitation sequence (ChIP-seq) analysis on whole MCF7 cells using two different
218 importin α1 antibodies. Comparison of the ChIP-seq data for importin α1 with a commercially
219 available dataset for modified histones revealed that importin α1 associated with euchromatin
220 regions characterized by H3K4me3 and H3K36me3, but not in heterochromatin regions marked
221 by H3K27me3 and H3K9me3 (Fig. 4C: represented chromosome 16, and Fig. 4D).

222 Taken together, our data indicate a preferential distribution of importin α1 in the
223 euchromatic areas rather than in the heterochromatic regions of MN.

224

225 **Search for potential importin α1-interacting proteins accumulated in MN**

226 Given that importin α1 is concentrated in euchromatin regions, likely due to its chromatin binding
227 capacity, we attempted to identify potential importin α1-interacting partners. To achieve this, we

228 performed rapid immunoprecipitation mass spectrometry of endogenous proteins (RIME) using
229 whole MCF7 cells (Mohammed *et al*, 2016). Using two independent samples from MCF7 cells,
230 we identified 102 proteins as potential importin α1 interactors which were excluded 4 overlapping
231 proteins (as shown 106 proteins in Fig. 5A and Table S1). Gene ontology analysis using the
232 PANTHER Pathways database (Mi *et al*, 2013; Thomas *et al*, 2022) revealed that many of these
233 proteins are involved in DNA replication and p53 pathways related to the DNA damage response
234 (Fig. 5B).

235 To narrow down the candidates implicated in MN localization, we screened the proteins
236 based on their localization using the online database Human Protein Atlas (HPA) database (Pontén
237 *et al*, 2008; Thul *et al*, 2017). Careful review of IF images in the HPA dataset revealed 60 proteins
238 that appeared in MN as well as PN. Out of twenty candidate MCF7 cell proteins identified by IF
239 analysis, eight proteins—CCAR2/DBC1, TOP2B, SUPT16H, PARP1, GTF2I, HDAC1, HDAC2,
240 and DNAJB1—were indeed detected within MN (Fig. 5C). Notably, the signals for
241 CCAR2/DBC1, TOP2B, SUPT16H, and PARP1 overlapped significantly with importin α1
242 signals from MN (Table S2). Additionally, the mCherry–PARP1 fusion protein colocalized with
243 EGFP–importin α1 in MN (Fig. 5D).

244 These results indicate the existence of the chromatin associated proteins that colocalize
245 with importin α in MN.

246

247 **Remarkably low mobility of importin α1 in the MN**

248 Interactions with chromatin via various proteins in MN may affect the molecular dynamics of
249 importin α1. To assess the mobility of importin α1 in MN, we analyzed reversine-treated HeLa
250 cells expressing EGFP–importin α1 using fluorescence recovery after photobleaching (FRAP).
251 The mobility of importin α1 was remarkably lower in MN than in PN (Fig. 6A-C). Moreover, we

252 found that three distinct modes of mobility were observed, namely, high, middle, and low. These
253 results indicate that the dynamics of MN-localized importin α1 differ from those of a canonical
254 nuclear transport factor.
255
256 **Mutually exclusive MN localization of importin α1 and RAD51**
257 In our investigation of importin α1-intereacting partners and their roles in MN, we discovered that
258 RAD51, a homologous recombination repair protein involved in DNA damage response,
259 accumulated in the MN of etoposide-treated HeLa cells (Fig. 7A). Up to 43% of the MN exhibited
260 RAD51-positive signals (Fig. 7B). Although most RAD51-positive MN displayed low-intensity
261 signals (Fig. 7C, upper panels: Cell #1, white arrowhead), a small subset of MN occasionally
262 showed significantly stronger fluorescence intensity (Fig. 7C, lower panels: Cell #2, yellow
263 arrowhead).
264 Notabley, we found that the localization of importin α1 and RAD51 in MN was mutually
265 exclusive. MN with low RAD51 signal intensity exhibited strong importin α1 signal intensity (Fig.
266 7D, upper panels: Cell #1, yellow arrowhead), and vice versa (Fig. 7D, lower panels: Cell #2,
267 white arrowhead). Moreover, these molecules exhibited distinct compartmentalization while
268 localizing in MN in a single cell (Fig. 7E, Cells #1 and #2: yellow arrowhead; importin α1-positive
269 and RAD51-negative MN, white arrowhead; importin α1-negative and RAD51-positive MN).
270 Finally, the signal intensity of endogenous RAD51 was remarkably low in MN overexpressing
271 EGFP–importin α1 (Fig. 7F, and 7G). Importantly, such altered distribution was not observed for
272 one of the binding candidates, PAPR1(Fig. 5D), indicating that the mutual exclusion was specific
273 to RAD51.
274 Taken together, these data suggest that highly enriched importin α1 in MN inhibits the
275 RAD51 accessibility, highlighting the role of importin α in modulating the MN state by

276 influencing both importin α-associated chromatin proteins and those excluded from the importin

277 α-enriched MN.

278 **DISCUSSION**

279 In this study, we found that several subtypes of importin α were localized in MN of human cancer
280 cells, indicating that the MN localization is a common feature of the importin α proteins. Notably,
281 importin α localized in some MN but not in others. This observation suggests that specific features
282 of the MN state, such as its structure and function, may be related to the unique function of
283 importin α.

284 MN localization of importin α1 did not fully correlate with the cellular distribution of
285 importin α-related transport factors, such as importin β1, CAS/CSE1L, and Ran, and with the
286 transport of cNLS substrates into MN. Furthermore, all tested EGFP–importin α1 mutants (ΔIBB,
287 ED, and C-mut), which do not exhibit nuclear transport functions, showed MN localization.
288 Further, C-mut, which is defective in nuclear export, localized in both PN and MN, whereas wild-
289 type importin α1 was observed exclusively in MN. These results suggest some differences in the
290 nucleocytoplasmic recycling of importin α1 in PM and MN. In particular, importin α1 is rapidly
291 recycled from PN, whereas it moves very slowly between MN and the cytoplasm. This
292 observation indicates that nuclear export of importin α1 from MN is disrupted or inhibited. We
293 hypothesize that interaction with some components, such as the chromatin-regulating proteins
294 identified in this study, suppresses the nuclear export of importin α from MN, leading to
295 significant accumulation.

296 The high concentration of importin α in MN may have also resulted in nuclear envelope
297 defects. We have demonstrated herein that importin α1 was enriched in the lamin-deficient areas
298 of MN, as evidenced by electron microscopy analysis showing a fragile morphology of the nuclear
299 envelope. We therefore propose that importin α1 mediates the construction and/or collapse of the
300 nuclear envelope of MN. A previous study demonstrated that exogenously added recombinant
301 importin α proteins inhibited nuclear envelope assembly around decondensed sperm chromatin in

302 *Xenopus* egg extracts (Hachet *et al*, 2004), indicating that highly concentrated importin α inhibits
303 nuclear membrane formation. An alternative scenarios that cannot be ruled out is that importin α
304 accumulation is not the cause of nuclear membrane collapse, but rather a consequence of it.
305 Emerging research indicates that interactions between mitochondria and MN may induce nuclear
306 envelope damage and/or inhibit the repair of nuclear membrane defects, possibly via reactive
307 oxygen species generated by mitochondria located near MN (Di Bona *et al*, 2024; Martin *et al*,
308 2024). Although we did not collect data on the proximity of importin α-positive MN to
309 mitochondria in this study, our findings suggest alternative mechanisms that may promote nuclear
310 membrane damage or impede the repair of membrane defects in MN.

311 Ruptured MN are associated with chromothripsis and innate immunity mediated by the
312 cyclic GMP–AMP synthase–stimulator of interferon genes (cGAS-STING) pathway, both of
313 which play critical roles in tumorigenesis, senescence, inflammation, and cancer immunotherapy
314 (Guo *et al.*, 2020; Guo *et al*, 2022; Kirsch-Volders *et al*, 2020). In this context, our study highlights
315 the underappreciated role of importin α in cancer processes, particularly through its effects when
316 enriched within MN. In a previous study, we demonstrated that nuclear-localized importin α
317 associates with DNase-sensitive chromatin components and is involved in gene regulation
318 (Yasuda *et al.*, 2012). We further reported that genetic loss of importin α4 (KPNA4) in mice leads
319 to changing the epigenetic status of chromatin, which is associated with abnormal sperm
320 formation and brain inflammation (Miyamoto *et al.*, 2020; Sakurai *et al*, 2024). Furthermore,
321 research shows that importin α binds to DNA through the IBB domain (Jibiki *et al.*, 2021). These
322 findings, along with those of this study regarding the distribution of importin α1 in conjunction
323 with histone modification markers and its notably slow mobility in MN, interestingly demonstrate
324 the ability of importin α to directly associate with DNA/chromatin fibers through some
325 components in MN, with potential implications for the induction of the chromothripsis process

326 and regulation of the cGAS-STING pathway in cancer cells.

327 Finally, we have provided evidence for an unrecognized molecular connection between
328 importin α1 and RAD51 in MN. Although RAD51 was not initially identified as a binding partner
329 in the RIME analysis, a previous study noted importin α1 (referred to as importin α2) as a
330 component of the RAD51 complex with CAS/CSE1L (Okimoto *et al*, 2015). This finding
331 suggests a potential role for importin α1 in regulating DNA repair processes related to RAD51,
332 which is vital for preventing mutations and maintaining genomic stability (Wassing & Esashi,
333 2021). Increased RAD51 expression is associated with enhanced recombination events and
334 genome instability in tumor cells (Klein, 2008; Richardson *et al*, 2004). Both importin α1 and
335 RAD51 have been implicated in tumorigenesis and patient survival (Christiansen & Dyrskjot,
336 2013; Han & Wang, 2020; Liao *et al*, 2022). Therefore, the enrichment of importin α1 in MN,
337 along with its interaction with the chromatin, may regulate the accessibility of RAD51 to
338 DNA/chromatin fibers in MN and protect its activity. This is supported by the observation that
339 breast cancer tissues that highly express importin α1 exhibit the cytoplasmic localization of
340 RAD51 (Alshareeda *et al.*, 2015). Understanding the regulatory mechanism and consequences of
341 RAD51 exclusion by importin α1 in MN is essential for gaining deeper insights into genome
342 instability, which promotes cancer progression and malignancy.

343 In summary, our results reveal that importin α is uniquely distributed and alters the
344 nuclear/chromatin status when enriched in MN. This finding indicates that importin α can serve
345 as a molecular marker for characterizing the dynamics of MN (Fig. 8). These discoveries will be
346 valuable for researchers interested in exploring the heterogeneity, quality control, and fate of MN
347 in various cellular processes, including tumorigenesis, senescence, inflammation, and cancers
348 immunotherapy.

349 **MATERIALS AND METHODS**

350 **Cell lines and culture conditions**

351 Human cervical cancer cell line HeLa cells were obtained from the RIKEN cell bank (Tsukuba,
352 Japan). Human breast cancer cell line MCF7 was obtained from NIBIOHN (JCRB 0134), and
353 MDA-MB-231, SK-BR-3, and human breast epithelial cell line MCF10A were kindly gifted from
354 Satoshi Fujii (National Cancer Center, Japan). HeLa and SK-BR-3 cells were maintained in
355 Dulbecco's Modified Eagle's Medium (DMEM; Sigma-Aldrich, St. Luis, MO) containing 10%
356 fetal bovine serum (FBS). MCF7 cells were maintained in Minimum Essential Medium (MEM)
357 Alpha no phenol red (Life Technologies, Carlsbad, CA) containing 10 % FBS, 0.1 mM MEM
358 Non-essential amino acids (NEAA; Life Technologies), 1 mM Sodium pyruvate (Life
359 Technologies), and 10 μg/mL Insulin (Wako, Osaka, Japan). MDA-MB-231 cells were cultured
360 in the RPMI1640 medium (Sigma-Aldrich) containing 10 % FBS and 2 mM L-Glutamine (Life
361 Technologies). MCF10A cells were cultured in MEG mammary epithelial cell growth medium
362 BulletKit added to SingleQuote (CC-3150) and 10 % FBS. Cells were cultured at 37 °C in a 5%
363 CO2 incubator. Reversine (Cayman Chemical, MI, USA) and etoposide (Tokyo Chemical
364 Industry (TCI) Co., LTD., Tokyo, Japan) were used as described in Fig. S2A-D and Fig. 7A.

365

366 **Antibodies**

367 Primary antibodies used in the experiments are listed in Table S3. The secondary antibodies used
368 were: Alexa Fluor Plus 488 (A32723, A32790, A32731, and A32814; Thermo Fisher Scientific
369 Inc, Rockford, IL, USA), and Alexa Fluor 488 (A11055), Alexa Fluor 594 (A-21203, A32754, and
370 A11032) for an indirect IF and horseradish peroxidase (HRP)-conjugated anti-goat, anti-rabbit, or
371 anti-mouse secondary antibodies (Jackson ImmunoResearch Inc West Grove, PA, USA) for
372 western blotting.

373

374 **Immunofluorescence analysis**

375 MCF7, MDA-MB-231, and HeLa cell lines were cultured on 18 × 18 mm coverslips (Menzel-
376 Glaser, Braunschweig, Germany) in a 35 mm dish, and immunofluorescence analysis was
377 performed as follows. Cells were fixed with 3.7% formaldehyde in phosphate-buffered saline
378 (PBS) for 15 min, followed by treatment with 0.5% Triton X-100 in PBS for 5 min. After blocking
379 with 3% skim milk in PBS for 30 min at 25 °C, the cells on the coverslips were labeled with
380 primary antibodies overnight and following by reacted with secondary antibodies accordingly for
381 1 h at 25 °C. To visualize DNA, the slides were incubated with DAPI (1:5000 in PBS, Dojindo)
382 for 20 min. The fluorescence images were observed using a confocal microscope (Leica TCS SP8
383 II; Leica Microsystems, Wetzlar, Germany).

384

385 **Plasmid construction for mammalian expression**

386 Human importin α1 (KPNA2) cDNA subcloned into the pGEX6P2 plasmid was gifted from Akira
387 Tsujii (NIBIOHN) and then cloned into pEGFPC1 vector (Clontech, Mountain View, CA, USA).
388 Plasmids for pEGFP-mouse importin α1 (KPNA2) was constructed as described previously
389 (Yasuda *et al.*, 2012). The SV40T antigen NLS (NLS; PKKKRKVED) within pmCherry-C1
390 (pmCherry–NLS) was constructed as described (Miyamoto *et al*, 2022). The pEGFPC1-NES
391 plasmid was kindly gifted from Dr. Asally (Asally *et al*, 2011). The cDNAs encoding PARP1 and
392 RAD51 were amplified from HeLa cells by PCR using the following primers: PARP1 forward:
393 5'-GTCCGGACTCAGATCTATGGCGGAGTCTTCGGAT-3' and 5'-
394 CCGCGGTACCGTCGACTTACCACAGGGAGGTCTTA-3', and RAD51 forward: 5'-
395 GTCCGGACTCAGATCTATGGCAATGCAGATGCAGCT-3' and reverse: 5'-
396 CCGCGGTACCGTCGACTCAGTCTTTGGCATCTCCCACT-3'. The cDNAs were cloned into

397 the pmCherryC1 vector using an In-Fusion HD cloning kit (Clontech, Mountain View, CA, USA).

398

399 **Transfection**

400 HeLa cells were plated onto 18 × 18 mm coverslips (Menzel-Glaser) in a 35 mm dish 2 days prior
401 to transfection. The transfections for mammalian expression plasmids were performed using
402 Lipofectamine 2000 DNA Transfection Reagent (Thermo Fisher Scientific) following the
403 manufacturer's instructions.

404

405 **Western blotting**

406 Western blotting was performed as previously described (Miyamoto *et al.*, 2022). Twenty ug of
407 whole cell lysates were subjected to 10% Supersep SDS-PAGE gel (Wako, Osaka, Japan). The
408 membranes were incubated with primary antibodies (dilutions ranging from 1:2000) diluted in
409 Can Get Signal Immunoreaction Enhancer Solution 1 (TOYOBO, Osaka, Japan) overnight at 4 °C.
410 The used HRP-conjugated secondary antibodies (dilutions ranging from 1:8000 to 1:10,000) were
411 diluted in Can Get Signal Immunoreaction Enhancer Solution 2 (TOYOBO) at 25 °C for 1 h. The
412 signals were detected with ATTO EzWest lumi plus (WSE-7120S, ATTO Corporation, Tokyo,
413 Japan).

414

415 **Correlative light-electron microscopy (CLEM)**

416 CLEM analysis was performed as described previously (Yokota *et al*, 2021), with some
417 modifications. Briefly, HeLa cells attached on gridded coverslips (Matsunami) were transfected
418 with pEGFP-human importin α1 (KPNA2) for 1 day and treated with 400 nM reversine. Then, the
419 cells were fixed in 2% paraformaldehyde, 0.5% glutaraldehyde, and 50 mM sucrose in 0.1 M
420 phosphate buffer, and stained with Hoechst 33342 for 1 h. After taking bright field and

421 fluorescence images using a BZ-X810 microscope (KEYENCE, Osaka, Japan), the cells were
422 further fixed in 2% glutaraldehyde and 50 mM sucrose in 0.1 M phosphate buffer, and post-fixed
423 with 1% osmium tetroxide. Fixed cells were dehydrated and embedded in Epok 812 (Oken Shoji).
424 Ultrathin sections were cut using a UC6 ultramicrotome (Leica), stained with uranyl acetate and
425 lead citrate, and examined using a JEM-1400 electron microscope (JEOL).
426
427 **Chromatin immunoprecipitation sequence (ChIP-seq)**
428 MCF7 cells (1×10^6) were grown in 100 mm dishes (IWAKI, Tokyo, Japan) for 7 days, and fixed
429 at 25 °C for 5 min by adding 135 μL of 37% formaldehyde solution (Nacalai tesque) in 10 mL of
430 the culture medium. Fixed cells were washed twice with ice-cold PBS twice and collected with
431 0.5 mL of ice-cold PBS using a cell lifter (Corning, NY), and centrifuged at 600 ×g at 4 °C for 5
432 min. The cells were resuspended in ChIP buffer [10 mM Tris-HCl (pH 8.0), 200 mM KCl, 1 mM
433 $CaCl_2$, 0.5% NP40] containing a protease inhibitor cocktail (No.25955, Nacalai tesque), briefly
434 sonicated (Branson 250 Sonifier, Branson Ultrasonics), and incubated on ice for 10 min. After
435 centrifugation at 10,000 ×g at 4 °C for 10 min, the supernatants were digested with 1 U/mL
436 micrococcal nuclease (Worthington Biochemical) at 37 °C for 30 min. The reaction was stopped
437 with EDTA (final concentration of 10 mM), and centrifuged at 10,000 ×g at 4 °C for 10 min. The
438 supernatants were incubated with anti-rabbit or anti-mouse IgG magnetic beads (Dynabeads, Life
439 Technologies) with anti-importin α1 (BD Biosciences, Cat. #610486; Abcam, Cat. # ab84440,
440 Table S3) for 8 h. The beads were washed twice with ChIP buffer, ChIP wash buffer [10 mM Tris-
441 HCl (pH 8.0), 500 mM KCl, 1 mM $CaCl_2$, 0.5% NP40, a protease inhibitor cocktail], and TE
442 buffer [10 mM Tris-HCl (pH 8.0) and 1 mM EDTA] and eluted overnight in an elution buffer
443 containing [50 mM Tris-HCl (pH 8.0), 10 mM EDTA, and 1% sodium dodecyl sulfate (SDS)] at
444 65 °C. DNA was recovered using AMPure XP beads (Beckman Coulter) and used for preparation

445 for ChIP-seq analysis.

446 A ChIP library was prepared using the NEBNext Ultra DNA Library Prep Kit for
447 Illumina (New England Biolabs) following the manufacturer's instructions, and sequencing was
448 conducted on an Illumina HiSeq1500 system. Sequence reads were aligned to the reference human
449 genome (GRCh38) using Hisat2 (version 2.0.5). Genomic tracks (bigWig) and correlation matrix
450 were generated using deepTools (version 3.4.5).

451

452 **Rapid immunoprecipitation mass spectrometry of endogenous proteins (RIME)**

453 MCF-7 cells (1.5×10^6) were cultured in 100 mm dishes (IWAKI) in 10 mL of MEM medium
454 with 10% FBS for 5 days. To fix the cells, 1/10 volume (1 mL) of freshly prepared Formaldehyde
455 Solutions [FS: 11% Methanol free formaldehyde, 0.1 M NaCl, 1 mM EDTA, and 50 mM Hepes
456 (pH7.9)] was directly added to the medium and incubated for 8 min at 25 °C. After the addition
457 of 0.55 mL 2.5 M glycine solution to the 11 mL of the medium (final conc. 0.1 M) to quench
458 crosslinking for 5 min, cells were washed twice with ice-cold PBS. After removal of the
459 supernatants, cells were collected at 800 × *g* for 10 min at 4 °C, and then, the cell pellets were
460 resuspended with 10 mL of ice-cold PBS with 0.5% Igepal CA-630 (#I-8896, Sigma-Aldrich) and
461 then centrifuged again. The cell pellets were suspended with 10 mL of ice-cold PBS with 0.5%
462 Igepal CA-630 and 100 μL of 100 mM Phenylmethylsulfonyl fluoride (PMSF) in EtOH (final
463 conc. 1 mM). The cell suspension was centrifuged thrice to pellet the cells, and then, the cell
464 pellets were snap-frozen in liquid N2 and stored at -80 °C. RIME analysis was performed by
465 Active Motif, CA., according to published protocols (Mohammed *et al.*, 2016). RIME was carried
466 out using an antibody against importin α1 (KPNA2; Ab2 in Table S3) and 150 μg of chromatin
467 from MCF7 cells to identify proteins that interact with importin α1 using mass spectrometry.
468 Mass spectrometry of the immunoprecipitated protein complexes resulted in 57–60% coverage of

469 importin α1.

470

471 **Fluorescence recovery after photobleaching (FRAP)**

472 HeLa cells (ATCC, CCL-2.2) were cultured in DMEM supplemented with 10 % FBS at 37 °C
473 under 5 % CO_2. A plasmid encoding EGFP–human importin α1(KPNA2) was introduced into
474 HeLa cells with polyethyleneimine (Polyscience, 49553937). The cells were replated onto a glass-
475 bottom dish (D11130H, Matsunami) 12 h after transfection and incubated for another 12 h. The
476 cells were further incubated in the presence of reversine (400 nM) for 20 h. Fluorescence
477 observation and FRAP analysis were performed using confocal laser scanning microscopy
478 (Evident, FV3000). Time-lapse images of green fluorescence were obtained every 10 sec for 6
479 min (for micronuclei) or every 3 sec for 1 min (for primary nuclei). Between 3rd and 4th images,
480 the fluorescence signal of a region of interest (ROI) was bleached by 488 nm laser irradiation.
481 The fluorescence signals of ROI was quantified using Image J (ver.1.54f).

482

483 **Accession number**

484 The ChIP-Seq data are accessible through GEO Series accession number GSE283000.

485

486 **Statistical analysis**

487 Cells and MN were counted optically under a microscope using the appropriate fluorescence field.
488 Unless stated otherwise, all data are presented as the mean ± standard deviation (s.d.). Within
489 individual experiments, data points were based on a minimum of triplicate representative samples.
490 Data were analyzed with Prism 9.0 software (GraphPad Software, La Jolla, CA).

ACKNOWLEDGMENTS

We thank Akira Tsujii (NIBIOHN) for kindly gifting the pGEX6P2-human importin α1 plasmid, Munehiro Asally (University of Warwick) for kindly gifting the pEGFPC1-NES plasmid, and Satoshi Fujii (National Cancer Center, Japan) for kindly gifting the human breast epithelial cells. We also thank the members of the Oka, Katagiri, and Saitoh Laboratories for their helpful discussion and technical support, and the Laboratory of Morphology and Image Analysis, Biomedical Research Core Facilities, Juntendo University Graduate School of Medicine for technical assistance.

FUNDING

This work was supported by Japan Society for the Promotion of Science (JSPS) KAKENHI grant numbers JP20K06455, JP22KK0111, and JP24K09446 to Y.M., JP17H01878 to H.S., and JP22H04926, Grant-in-Aid for Transformative Research Areas – Platforms for Advanced Technologies and Research Resources "Advanced Bioimaging Support", and The Naito Foundation (Japan) to H.S.

COMPETING INTERESTS

No competing interests declared.

AUTHOR CONTRIBUTIONS

YM and HS conceived originally the project, and designed the experiments. YM, RK, RO, SHY, MY, KM, CH, TT, MK, and YO performed the experiments. YM, RK, SHY, MY, KM, MK, YO, TK, YY, MO, and HS analyzed the data and designed figures. YM and HS wrote the manuscript.

514 **FIGURE LEGENDS**

515 **Figure 1. Accumulation of importin α proteins in MN.** (A) Western blot analysis using specific
516 antibodies to detect importin α (Imp-α/KPNA) subtypes, importin β1 (Imp-β1/KPNB1),
517 CAS/CSE1L, and ACTIN as a loading control in whole cell extracts from a human breast
518 epithelial cell line (MCF10A) and breast cancer cell lines (MCF7, MDA-MB-231, and SK-BR-
519 3). An antibody against importin α1 (KPNA2) was used the Ab2 in Table S3. (B) An indirect IF
520 analysis for MCF7 cells using an anti-importin α1 antibody (Imp-α1). The left enlarged image is
521 extracted from the area enclosed by the red dotted line in the right image. Yellow arrowhead shows
522 high intensity of importin α1 signals in MN. DNA is stained with DAPI. Bar = 30 μm. (C) IF
523 image of importin α1 in HeLa cells. Yellow arrowhead: high intensity of importin α1 signals in
524 MN. White dotted lines indicate cellular boundaries. DNA is stained with DAPI. The yellow line
525 described with X and Y is for fluorescence intensity that is showed in D. (D) Fluorescent
526 intensities of importin α1 (green) and DAPI (blue) are measured along with the X-Y line
527 represented in C. PN: primary nucleus, MN: micronucleus. (E) Representation of overexpressed
528 EGFP–importin α1 (EGFP-Imp-α1) in HeLa cells which are treated with reversine for 20 h. PN:
529 primary nuclei (upper panels), MN: micronuclei (middle panels), both of PN and MN (PN/MN,
530 lower panels). DNA is stained with Hoechest33342. Yellow arrowheads or white arrows indicate
531 MNs with either high intensity or no intensity of EGFP–Imp-α1. Bar = 20 μm. (F) The ratio of
532 EGFP–Imp-α1 localized in either PN, MN or PN/MN, exhibited in E. The number of Hoechst-
533 stained cells (approximately 35 cells per an observed area) is counted to derive the percentage of
534 either the EGFP–Imp-α1 positive PN, MN or PN/MN. Data are representative of three
535 independent experiments (108 cells in total).

536

537 **Figure 2. Localization of the nuclear transport factors and cNLS-substrates in importin α1-**

538 **enriched MN.**

539 (A) Indirect IF images of importin α1 with either importin β1, CAS/CSE1L and Ran in reversine-
540 treated HeLa cells. DNA is stained with DAPI. White dotted lines indicate cellular boundaries.
541 Yellow arrowhead: high intensity of importin α1 signals, white arrow: no intensity of importin α1
542 signals. Bar = 10 μm. (B) Ratio of MN localization of either importin β1, CAS/CSE1L, or Ran
543 against the total number of MN in reversine-treated HeLa cells. The number of DAPI-stained MN
544 is counted for independent experiments as shown in A (n=4, 80 cells in total each). (C) Ratio of
545 MN localization of either importin β1, CAS/CSE1L, or Ran against the importin α1-positive MN
546 in reversine-treated HeLa cells (n=4, 80 cells in total each). (D) Indirect IF images of MN
547 localized importin-α1 in mCherry–NLS-expressing HeLa cells with reversine treatment. Yellow
548 arrowheads: Imp-α1-positive MN, white arrows: Imp-α1-negative MN. (E) Ratio of MN
549 localization of importin α1 against the NLS-positive- or NLS-negative MN as shown in D (n=4,
550 170 cells in total).

551

552 **Figure 3. Nuclear envelope collapse of importin-α1-enriched MN.**

553 (A–B) Indirect IF images of importin α1 with lamin B1 (A) or lamin A/C (B) in reversine-treated
554 HeLa cells. Two images of an independent cell are shown in the upper panel (Cell #1), and the
555 lower panels show an enlarged MN image (Cell #2). The fluorescence intensities of importin α1
556 (green), Lamin B1 or Lamin A/C (red), and DAPI (blue) are measured along with the X-Y line in
557 the lower panel (Cell #2). Yellow arrowhead: high intensity of importin α1 signals, white arrow:
558 no importin α1 signals. Bar = 10 μm. (C) CLEM analysis of importin α1-expressing MN. Left
559 image: The merged EGFP–importin α1, Hoechst 33342, and TEM images of reversine-treated
560 HeLa cells. The boxed area indicates EGFP-positive MN. Scale bar = 5 μm. Center image:
561 enlarged TEM image of MN in the left box. Scale bar = 1 μm. Right image: enlarged TEM image

562 of the box in the center image. White arrowheads indicate an area lacking the inner and outer
563 nuclear membranes of the micronucleus. Scale bar = 500 nm. TEM: transmission electron
564 microscopy; PN: primary nucleus; MN: micronucleus. (D) MN localization of importin α1 and
565 lamin B1 in EGFP–NES-expressing HeLa cells treated with reversine. Two images of an
566 independent cell are shown in the upper (Cell #1) and the lower panels (Cell #2). Yellow
567 arrowheads: Imp-α1-positive MN, white arrows: Imp-α1-negative MN. (E) MN localization ratio
568 of EGFP–NES in Imp-α1-negative (left) and Imp-α1-positive (right) MN, measured per 10 cells
569 (4 observation regions, total >40 cells counted).
570
571 **Figure 4. Euchromatin localization of importin α1 in MN.**
572 (A–B) Indirect IF images of importin α1 with H3K4me3 (A) or H3K9me3 (B) in normally
573 cultured MDA-MB-231 cells. The upper enlarged images are extracted from the area enclosed by
574 the red dotted line in the lower image. DNA is stained with DAPI. Fluorescent intensities of
575 importin α1 (green), modified histones (red: H3K4me3 or H3K9me3), and DAPI (blue) in MN
576 are measured along with the X-Y line and represented in the left low. Bar = 10 μm. (C) Alignment
577 of ChIP-seq data for importin α1 and modified histones in whole MCF7 cells (chromosome 16 is
578 represented). Two independent importin α1 antibodies (Ab1 and Ab2 in Table S3) were used for
579 ChIP analysis and modified histones data was obtained from public data set of ENCODE project
580 (H3K4me3: ENCSR000DWJ, H3K27me3: ENCSR000EWP, H3K36me3: ENCSR000EWO,
581 H3K9me3: ENCSR000EWQ). (D) Plot the Spearman's correlation coefficient matrix for ChIP-
582 seq data for two independent importin α1 antibodies and modified histones in MCF7 cells.
583
584 **Figure 5. Exploration of importin α1-binding proteins through RIME.**
585 (A) Venn diagram grouping candidate importin α1-binding proteins by RIME. Two independent

586 experiments are performed. MCF7-R1 and MCF7-R2 are proteins precipitated by anti-importin
587 α1 antibodies, and IgG Control-R1 and -R2 are proteins precipitated by normal IgG antibodies.
588 One hundred and six proteins are candidate binding partners of importin α1. (B) Gene Ontology
589 analysis for identified binding proteins. All gene ontology terms are identified as a result of
590 querying the PANTHER Pathways database for the importin α1-interacting proteins identified by
591 RIME. Terms are ranked by p-value. (C) Indirect IF analysis of importin α1 with candidate
592 molecules identified by RIME in HeLa cells. Cells are treated with 400 nM reversine for 20 h,
593 and the molecules described are detected by the specific antibodies (Table S3). White dotted lines
594 indicate cellular boundaries. DNA is stained with DAPI. Merged images are shown on the right
595 side. The yellow arrowheads, white arrowheads, and white arrows indicate MN with either high
596 intensity, low intensity, or no intensity of importin α1, respectively. Bar = 20 μm. (D)
597 Overexpressed EGFP–importin α1 co-localizes with mCherry–PARP1 in HeLa cells. The yellow
598 arrowheads indicate MN with both proteins. Bar = 10 μm.
599
600 **Figure 6. FRAP analysis of EGFP–importin α1 in MN**. (A) Time-lapse images of EGFP–
601 importin α1 in MN and PN at the represented time points. The bleach area is indicated by the
602 yellow circle, which surrounds all MN or a part of PN. The enlarged images on the right were
603 extracted from the area enclosed by the red dotted line in the left image. Three types of recovery
604 modes are shown, namely, High, Middle, and Low. Bar = 10 μm. (B & C) Graphs representing
605 recovery kinetics data of FRAP analysis in panel A; the values are means for 6 MN (B) or 9 PN
606 (C). The FRAP curves were normalized to 100% using pre-bleaching values.
607
608 **Figure 7. Mutually exclusive localization of importin α1 and RAD51 in MN.**
609 (A) Schematic representation for reversine treatment followed by etoposide treatment to HeLa

610 cells. After 20 h treatment of 400 nM reversine, the cells are incubated with 10 μM etoposide for
611 6 h. (B) The ratio of the RAD51-positive MN against the DAPI-stained MN with or without
612 etoposide treatment. Signal intensities of 200 different cells in total from eight independent
613 experiments. **P < 0.01, two-tailed Student's t-test. error bars represent s.d. (C) Indirect IF
614 analysis of RAD51 in HeLa cells that are treated with reversine for 20 h followed by etoposide
615 for 6 h. Two images with independent cells are represented: the upper panels show MN with a
616 low signal intensity of RAD51 (Cell #1, white arrowhead), and the lower panels show MN with
617 a high signal intensity of RAD51 (Cell #2, yellow arrowhead). Bar = 10 μm. (D) Indirect IF
618 analysis of importin α1 with RAD51 in HeLa cells that are treated with reversine and followed
619 by etoposide. Two images with an independent cell are represented: the upper panels (Cell #1)
620 show MN with the high signal intensity of importin α1 (green) and low intensity of RAD51 (red,
621 yellow arrowhead), and the lower panels (Cell #2) show MN with the low signal intensity of
622 importin α1 and high signal intensity of RAD51 (white arrowhead). Bar = 10 μm. (E) Indirect IF
623 analysis of importin α1 with RAD51 in HeLa cells that are treated with reversine and followed
624 by etoposide. In the upper panels (Cell #1), the single cell that is indicated with a white dotted
625 line has two MN which indicate high signal intensity of importin α1 (green, yellow arrowhead)
626 and high signal intensity of RAD51 (red, white arrowhead). The middle panels (Cell #2) show
627 two MN in one cell. The below panels show enlarged images that are extracted from the area
628 enclosed by the red dotted line. The yellow arrowheads indicate MN with a high signal intensity
629 of importin α1 and low signal intensity of RAD51, and the white arrowheads indicate MN with
630 low intensity of importin α1 and high intensity of RAD51. Bar = 10 μm. (F) Indirect IF analysis
631 of RAD51 in HeLa cells which are overexpressed EGFP–importin α1 (EGFP–Imp-α1). The cells
632 are transfected with EGFP–Imp-α1 and followed by treatment with reversine and etoposide. Two
633 images with an independent cell are represented as Cell #1 and #2. DNA is stained with DAPI.

634 Yellow arrowheads indicate EGFP–Imp-α1 localized MN. The yellow line is described with X
635 and Y in the lower panels (Cell #2) that is for the fluorescence analysis in G. Bar = 10 μm. (G)
636 Fluorescence intensities of EGFP–Imp-α1 (green), RAD51 (red), and DAPI (blue) in MN are
637 measured along with the X-Y line in F.
638
639 **Figure 8. Schematic illustrating how importin α serves as an undescribed molecular marker**
640 **for characterizing the MN state.**
641 Importin α (Imp-α) is present in euchromatin of MN within human cancer cells. Its ability to
642 interact with a variety of nuclear proteins, including those involved in chromatin regulation,
643 suggests that it shapes the unique state of MN. Furthermore, certain proteins, such as RAD51, can
644 be excluded from such compartmentalization. Taken together, these findings suggest that
645 importin α plays a crucial role in regulating chromosome instability and cell fate in cancer cells.

REFERENCES

Agustinus AS, Al-Rawi D, Dameracharla B, Raviram R, Jones B, Stransky S, Scipioni L, Luebeck J, Di Bona M, Norkunaite D *et al* (2023) Epigenetic dysregulation from chromosomal transit in micronuclei. *Nature* 619: 176-183

Alshareeda AT, Negm OH, Green AR, Nolan CC, Tighe P, Albarakati N, Sultana R, Madhusudan S, Ellis IO, Rakha EA (2015) KPNA2 is a nuclear export protein that contributes to aberrant localisation of key proteins and poor prognosis of breast cancer. *Br J Cancer* 112: 1929-1937

Asally M, Yasuda Y, Oka M, Otsuka S, Yoshimura SH, Takeyasu K, Yoneda Y (2011) Nup358, a nucleoporin, functions as a key determinant of the nuclear pore complex structure remodeling during skeletal myogenesis. *FEBS J* 278: 610-621

Behrens P, Brinkmann U, Wellmann A (2003) CSE1L/CAS: its role in proliferation and apoptosis. *Apoptosis* 8: 39-44

Christiansen A, Dyrskjot L (2013) The functional role of the novel biomarker karyopherin α2 (KPNA2) in cancer. *Cancer Lett* 331: 18-23

Christie M, Chang CW, Róna G, Smith KM, Stewart AG, Takeda AA, Fontes MR, Stewart M, Vértessy BG, Forwood JK *et al* (2016) Structural Biology and Regulation of Protein Import into the Nucleus. *Journal of molecular biology* 428: 2060-2090

D'Alise AM, Amabile G, Iovino M, Di Giorgio FP, Bartiromo M, Sessa F, Villa F, Musacchio A, Cortese R (2008) Reversine, a novel Aurora kinases inhibitor, inhibits colony formation of human acute myeloid leukemia cells. *Molecular cancer therapeutics* 7: 1140-1149

Dahl E, Kristiansen G, Gottlob K, Klaman I, Ebner E, Hinzmann B, Hermann K, Pilarsky C, Durst M, Klinkhammer-Schalke M *et al* (2006) Molecular profiling of laser-microdissected matched tumor and normal breast tissue identifies karyopherin alpha2 as a potential novel prognostic marker in breast cancer. *Clin Cancer Res* 12: 3950-3960

Dankof A, Fritzsche FR, Dahl E, Pahl S, Wild P, Dietel M, Hartmann A, Kristiansen G (2007) KPNA2 protein expression in invasive breast carcinoma and matched peritumoral ductal carcinoma in situ. *Virchows Arch* 451: 877-881

Di Bona M, Chen Y, Agustinus AS, Mazzagatti A, Duran MA, Deyell M, Bronder D, Hickling J, Hong C, Scipioni L *et al* (2024) Micronuclear collapse from oxidative damage. *Science* 385: eadj8691

Fernandez-Martinez J, Rout MP (2021) One Ring to Rule them All? Structural and Functional Diversity in the Nuclear Pore Complex. *Trends Biochem Sci* 46: 595-607

Forment JV, Kaidi A, Jackson SP (2012) Chromothripsis and cancer: causes and consequences of chromosome shattering. *Nat Rev Cancer* 12: 663-670

Furuta M, Kose S, Koike M, Shimi T, Hiraoka Y, Yoneda Y, Haraguchi T, Imamoto N (2004) Heat-shock induced nuclear retention and recycling inhibition of importin α. *Genes Cells* 9:

682 429-441
683 Goldfarb DS, Corbett AH, Mason DA, Harreman MT, Adam SA (2004) Importin α: a
684 multipurpose nuclear-transport receptor. *Trends Cell Biol* 14: 505-514
685 Guo X, Dai X, Wu X, Zhou T, Ni J, Xue J, Wang X (2020) Understanding the birth of rupture-
686 prone and irreparable micronuclei. *Chromosoma* 129: 181-200
687 Guo X, Hintzsche H, Xu W, Ni J, Xue J, Wang X (2022) Interplay of cGAS with micronuclei:
688 Regulation and diseases. *Mutat Res Rev Mutat Res* 790: 108440
689 Hachet V, Kocher T, Wilm M, Mattaj IW (2004) Importin α associates with membranes and
690 participates in nuclear envelope assembly in vitro. *EMBO J* 23: 1526-1535
691 Hampoelz B, Andres-Pons A, Kastritis P, Beck M (2019) Structure and Assembly of the Nuclear
692 Pore Complex. *Annu Rev Biophys* 48: 515-536
693 Han Y, Wang X (2020) The emerging roles of KPNA2 in cancer. *Life Sci* 241: 117140
694 Hatch EM, Fischer AH, Deerinck TJ, Hetzer MW (2013) Catastrophic nuclear envelope collapse
695 in cancer cell micronuclei. *Cell* 154: 47-60
696 Hintzsche H, Hemmann U, Poth A, Utesch D, Lott J, Stopper H (2017) Fate of micronuclei and
697 micronucleated cells. *Mutat Res Rev Mutat Res* 771: 85-98
698 Jibiki K, Kodama TS, Suenaga A, Kawase Y, Shibazaki N, Nomoto S, Nagasawa S, Nagashima
699 M, Shimodan S, Kikuchi R *et al* (2021) Importin α2 association with chromatin: Direct DNA
700 binding via a novel DNA-binding domain. *Genes Cells* 26: 945-966
701 Kirsch-Volders M, Bolognesi C, Ceppi M, Bruzzone M, Fenech M (2020) Micronuclei,
702 inflammation and auto-immune disease. *Mutat Res Rev Mutat Res* 786: 108335
703 Klein HL (2008) The consequences of Rad51 overexpression for normal and tumor cells. *DNA*
704 *Repair (Amst)* 7: 686-693
705 Knockenhauer KE, Schwartz TU (2016) The Nuclear Pore Complex as a Flexible and Dynamic
706 Gate. *Cell* 164: 1162-1171
707 Kodiha M, Banski P, Ho-Wo-Cheong D, Stochaj U (2008) Dissection of the molecular
708 mechanisms that control the nuclear accumulation of transport factors importin-α and CAS in
709 stressed cells. *Cell Mol Life Sci* 65: 1756-1767
710 Krupina K, Goginashvili A, Cleveland DW (2021) Causes and consequences of micronuclei. *Curr*
711 *Opin Cell Biol* 70: 91-99
712 Kwon M, Leibowitz ML, Lee JH (2020) Small but mighty: the causes and consequences of
713 micronucleus rupture. *Exp Mol Med* 52: 1777-1786
714 Liao C, Talluri S, Zhao J, Mu S, Kumar S, Shi J, Buon L, Munshi NC, Shammas MA (2022)
715 RAD51 Is Implicated in DNA Damage, Chemoresistance and Immune Dysregulation in Solid
716 Tumors. *Cancers (Basel)* 14
717 Ly P, Cleveland DW (2017) Rebuilding Chromosomes After Catastrophe: Emerging Mechanisms

718 of Chromothripsis. *Trends Cell Biol* 27: 917-930
719 Maciejowski J, Hatch EM (2020) Nuclear Membrane Rupture and Its Consequences. *Annu Rev*
720 *Cell Dev Biol* 36: 85-114
721 Martin S, Scorzoni S, Cordone S, Mazzagatti A, Beznoussenko GV, Gunn AL, Di Bona M, Eliezer
722 Y, Leor G, Ben-Yishay T *et al* (2024) A p62-dependent rheostat dictates micronuclei
723 catastrophe and chromosome rearrangements. *Science* 385: eadj7446
724 Mi H, Muruganujan A, Thomas PD (2013) PANTHER in 2013: modeling the evolution of gene
725 function, and other gene attributes, in the context of phylogenetic trees. *Nucleic Acids Res* 41:
726 D377-386
727 Miller KN, Victorelli SG, Salmonowicz H, Dasgupta N, Liu T, Passos JF, Adams PD (2021)
728 Cytoplasmic DNA: sources, sensing, and role in aging and disease. *Cell* 184: 5506-5526
729 Miyamoto Y, Boag PR, Hime GR, Loveland KL (2012) Regulated nucleocytoplasmic transport
730 during gametogenesis. *Biochim Biophys Acta* 1819: 616-630
731 Miyamoto Y, Itoh Y, Suzuki T, Tanaka T, Sakai Y, Koido M, Hata C, Wang CX, Otani M, Moriishi
732 K *et al* (2022) SARS-CoV-2 ORF6 disrupts nucleocytoplasmic trafficking to advance viral
733 replication. *Commun Biol* 5: 483
734 Miyamoto Y, Saiwaki T, Yamashita J, Yasuda Y, Kotera I, Shibata S, Shigeta M, Hiraoka Y,
735 Haraguchi T, Yoneda Y (2004) Cellular stresses induce the nuclear accumulation of importin
736 α and cause a conventional nuclear import block. *J Cell Biol* 165: 617-623
737 Miyamoto Y, Sasaki M, Miyata H, Monobe Y, Nagai M, Otani M, Whiley PAF, Morohoshi A, Oki
738 S, Matsuda J *et al* (2020) Genetic loss of importin α4 causes abnormal sperm morphology and
739 impacts on male fertility in mouse. *Faseb j* 34: 16224-16242
740 Miyamoto Y, Yamada K, Yoneda Y (2016) Importin α: a key molecule in nuclear transport and
741 non-transport functions. *Journal of biochemistry* 160: 69-75
742 Mohammed H, Taylor C, Brown GD, Papachristou EK, Carroll JS, D'Santos CS (2016) Rapid
743 immunoprecipitation mass spectrometry of endogenous proteins (RIME) for analysis of
744 chromatin complexes. *Nat Protoc* 11: 316-326
745 Oka M, Yoneda Y (2018) Importin α: functions as a nuclear transport factor and beyond. *Proc Jpn*
746 *Acad Ser B Phys Biol Sci* 94: 259-274
747 Okimoto S, Sun J, Fukuto A, Horikoshi Y, Matsuda S, Matsuda T, Ikura M, Ikura T, Machida S,
748 Kurumizaka H *et al* (2015) hCAS/CSE1L regulates RAD51 distribution and focus formation
749 for homologous recombinational repair. *Genes Cells* 20: 681-694
750 Pontén F, Jirström K, Uhlen M (2008) The Human Protein Atlas--a tool for pathology. *J Pathol*
751 216: 387-393
752 Pumroy RA, Cingolani G (2015) Diversification of importin-α isoforms in cellular trafficking and
753 disease states. *Biochem J* 466: 13-28

754 Richardson C, Stark JM, Ommundsen M, Jasin M (2004) Rad51 overexpression promotes
755 alternative double-strand break repair pathways and genome instability. *Oncogene* 23: 546-
756 553
757 Sakurai K, Morita M, Aomine Y, Matsumoto M, Moriyama T, Kasahara E, Sekiyama A, Otani M,
758 Oshima R, Loveland KL *et al* (2024) Importin α4 deficiency induces psychiatric disorder-
759 related behavioral deficits and neuroinflammation in mice. *Transl Psychiatry* 14: 426
760 Santaguida S, Tighe A, D'Alise AM, Taylor SS, Musacchio A (2010) Dissecting the role of MPS1
761 in chromosome biorientation and the spindle checkpoint through the small molecule inhibitor
762 reversine. *J Cell Biol* 190: 73-87
763 Stewart M (2007) Molecular mechanism of the nuclear protein import cycle. *Nat Rev Mol Cell*
764 *Biol* 8: 195-208
765 Storchová Z, Kloosterman WP (2016) The genomic characteristics and cellular origin of
766 chromothripsis. *Curr Opin Cell Biol* 40: 106-113
767 Sun Y, Li W, Li X, Zheng H, Qiu Y, Yang H (2021) Oncogenic role of karyopherin α2 (KPNA2)
768 in human tumors: A pan-cancer analysis. *Comput Biol Med* 139: 104955
769 Thomas PD, Ebert D, Muruganujan A, Mushayahama T, Albou LP, Mi H (2022) PANTHER:
770 Making genome-scale phylogenetics accessible to all. *Protein Sci* 31: 8-22
771 Thul PJ, Åkesson L, Wiking M, Mahdessian D, Geladaki A, Ait Blal H, Alm T, Asplund A, Björk
772 L, Breckels LM *et al* (2017) A subcellular map of the human proteome. *Science* 356
773 Wang CI, Chien KY, Wang CL, Liu HP, Cheng CC, Chang YS, Yu JS, Yu CJ (2012) Quantitative
774 proteomics reveals regulation of karyopherin subunit alpha-2 (KPNA2) and its potential novel
775 cargo proteins in nonsmall cell lung cancer. *Mol Cell Proteomics* 11: 1105-1122
776 Wassing IE, Esashi F (2021) RAD51: Beyond the break. *Semin Cell Dev Biol* 113: 38-46
777 Wente SR, Rout MP (2010) The nuclear pore complex and nuclear transport. *Cold Spring Harb*
778 *Perspect Biol* 2: a000562
779 Yasuda Y, Miyamoto Y, Yamashiro T, Asally M, Masui A, Wong C, Loveland KL, Yoneda Y
780 (2012) Nuclear retention of importin α coordinates cell fate through changes in gene
781 expression. *EMBO J* 31: 83-94
782 Yokota M, Kakuta S, Shiga T, Ishikawa KI, Okano H, Hattori N, Akamatsu W, Koike M (2021)
783 Establishment of an in vitro model for analyzing mitochondrial ultrastructure in PRKN-
784 mutated patient iPSC-derived dopaminergic neurons. *Mol Brain* 14: 58
785 Zhang CZ, Spektor A, Cornils H, Francis JM, Jackson EK, Liu S, Meyerson M, Pellman D (2015)
786 Chromothripsis from DNA damage in micronuclei. *Nature* 522: 179-184

787

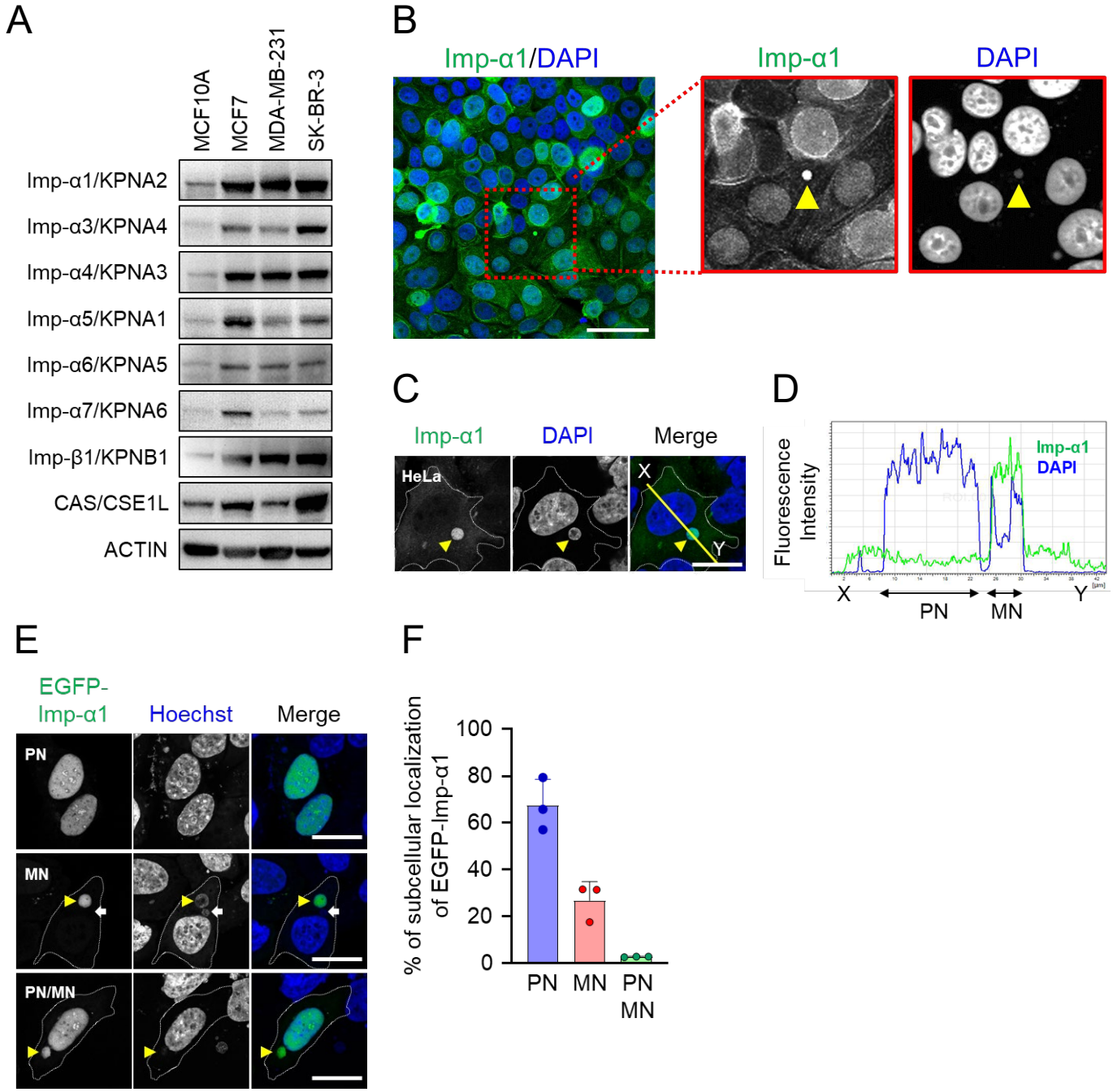
A
MCF10A
MCF7
MDA-MB-231
SK-BR-3
Imp-α1/KPNA2
Imp-α3/KPNA4
Imp-α4/KPNA3
Imp-α5/KPNA1
Imp-α6/KPNA5
Imp-α7/KPNA6
Imp-β1/KPNB1
CAS/CSE1L
ACTIN
B
Imp-α1/DAPI
Imp-α1
DAPI
C
Imp-α1
DAPI
Merge
HeLa
X
Y
D
Fluorescence Intensity
Imp-α1
DAPI
X
PN
MN
Y
E
EGFP-Imp-α1
Hoechst
Merge
PN
MN
PN/MN
F
% of subcellular localization of EGFP-Imp-α1
100
80
60
40
20
0
PN
MN
PN MN

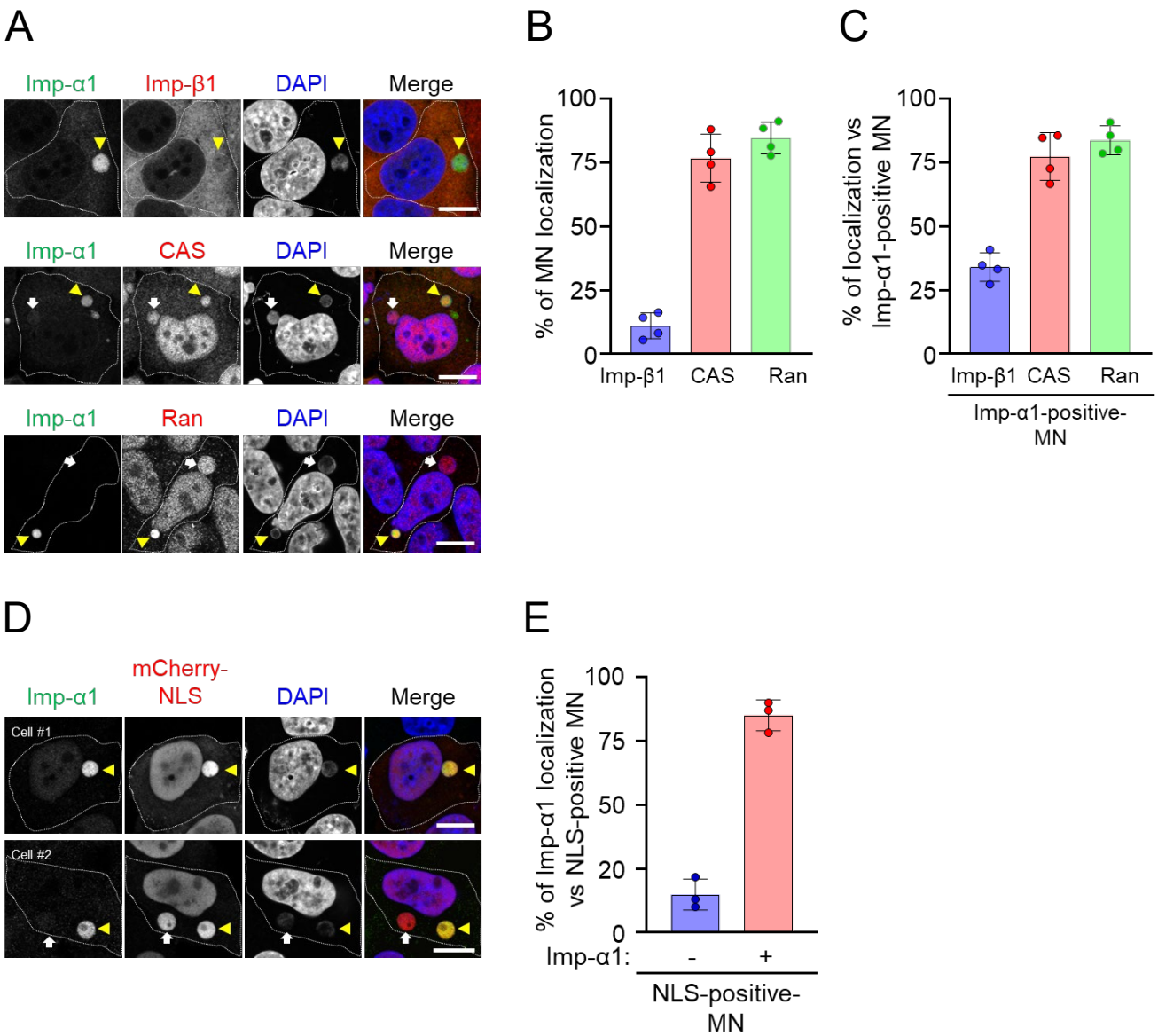
A
Imp-α1
Imp-β1
DAPI
Merge
Imp-α1
CAS
DAPI
Merge
Imp-α1
Ran
DAPI
Merge
B
% of MN localization
100
75
50
25
0
Imp-β1
CAS
Ran
C
% of localization vs Imp-α1-positive MN
100
75
50
25
0
Imp-β1
CAS
Ran
Imp-α1-positive-MN
D
Imp-α1
mCherry-NLS
DAPI
Merge
Cell #1
Cell #2
E
% of Imp-α1 localization vs NLS-positive MN
100
75
50
20
0
Imp-α1:
-
+
NLS-positive-MN

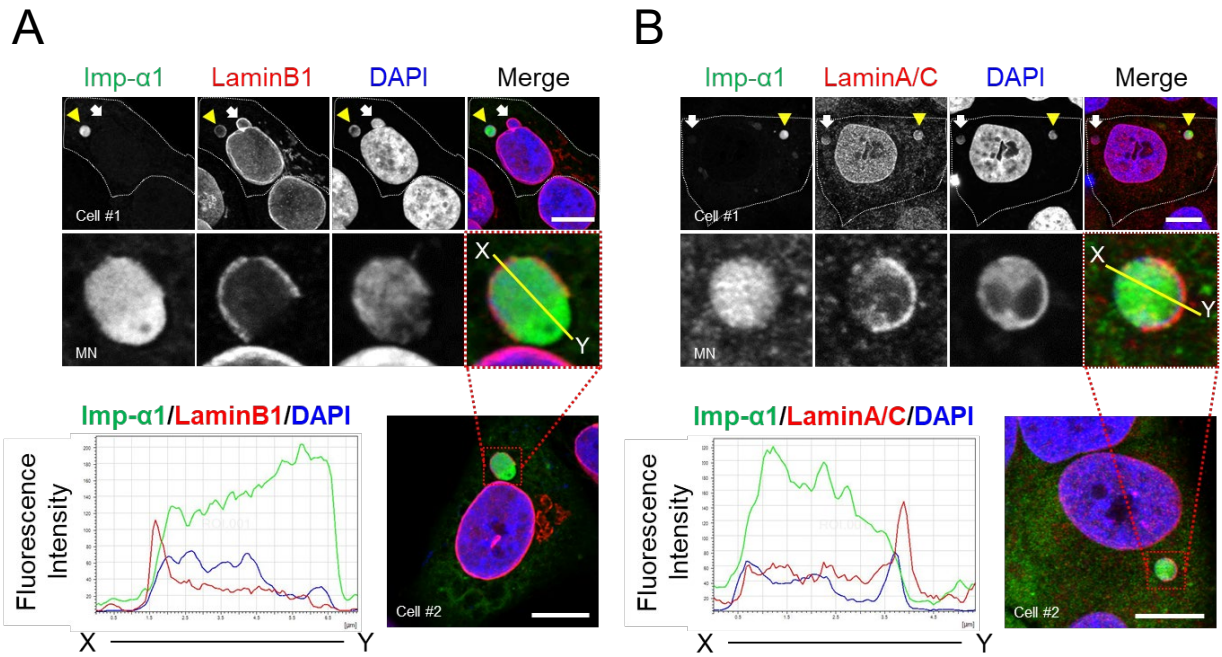
A
Imp-α1
LaminB1
DAPI
Merge
Cell #1
MN
X
Y
Imp-α1/LaminB1/DAPI
Fluorescence Intensity
Cell #2
B
Imp-α1
LaminA/C
DAPI
Merge
Cell #1
MN
X
Y
Imp-α1/LaminA/C/DAPI
Fluorescence Intensity
Cell #2

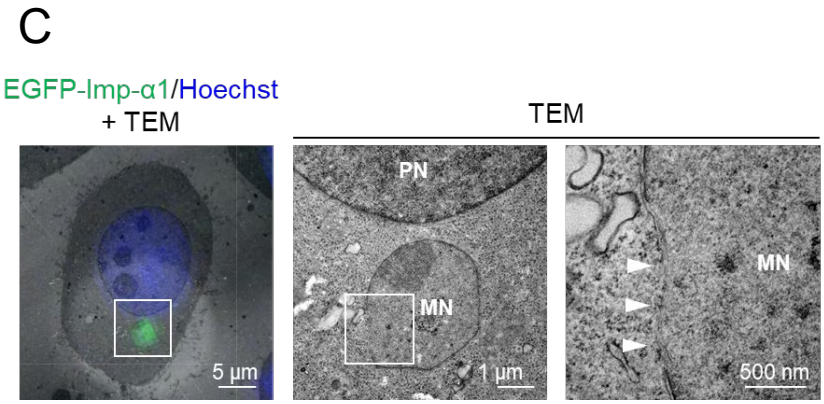
C
EGFP-Imp-α1/Hoechst
+ TEM
TEM
5 μm
PN
MN
1 μm
MN
500 nm

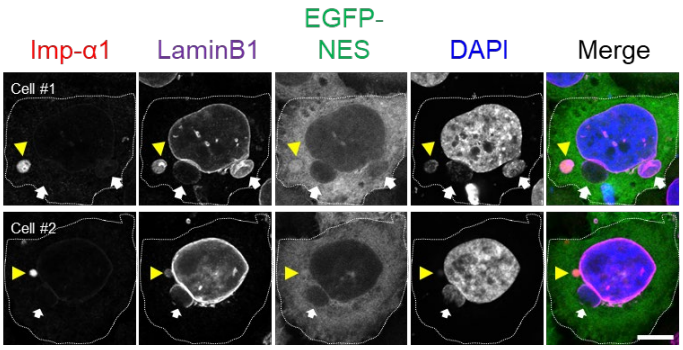
D
Imp-α1
LaminB1
EGFP-NES
DAPI
Merge
Cell #1
Cell #2

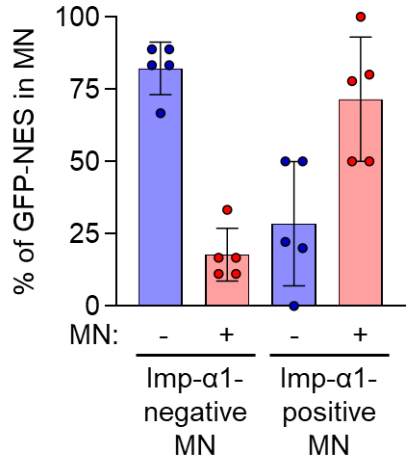
E
% of GFP-NES in MN
100
75
50
25
0
MN:
-
+
-
+
Imp-α1-negative MN
Imp-α1-positive MN

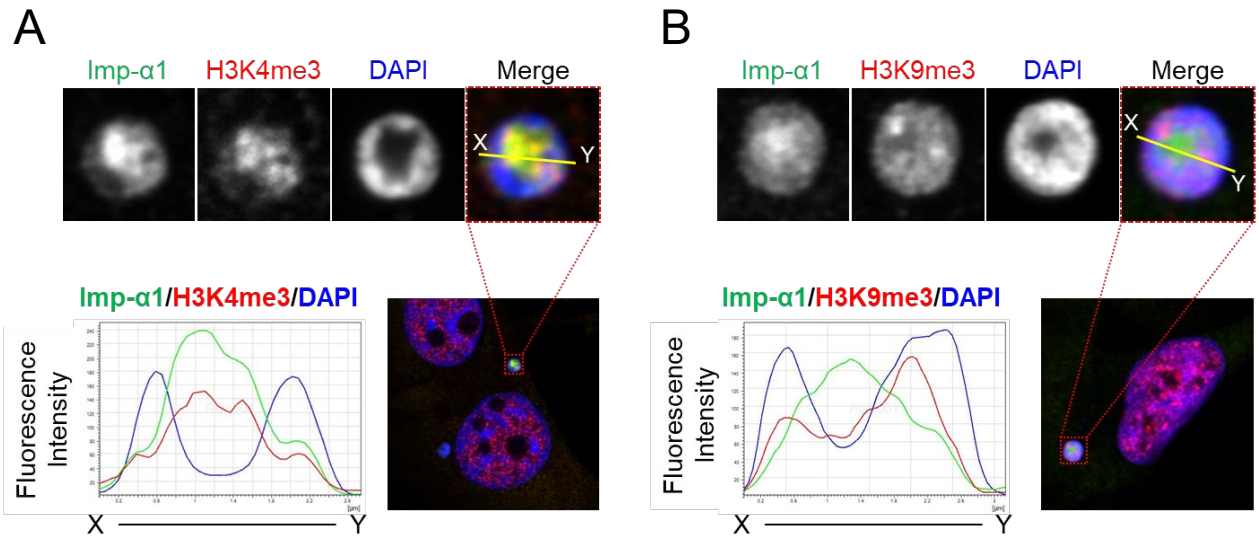
A
Imp-α1
H3K4me3
DAPI
Merge
X
Y
Imp-α1/H3K4me3/DAPI
Fluorescence Intensity
X
Y
B
Imp-α1
H3K9me3
DAPI
Merge
X
Y
Imp-α1/H3K9me3/DAPI
Fluorescence Intensity
X
Y

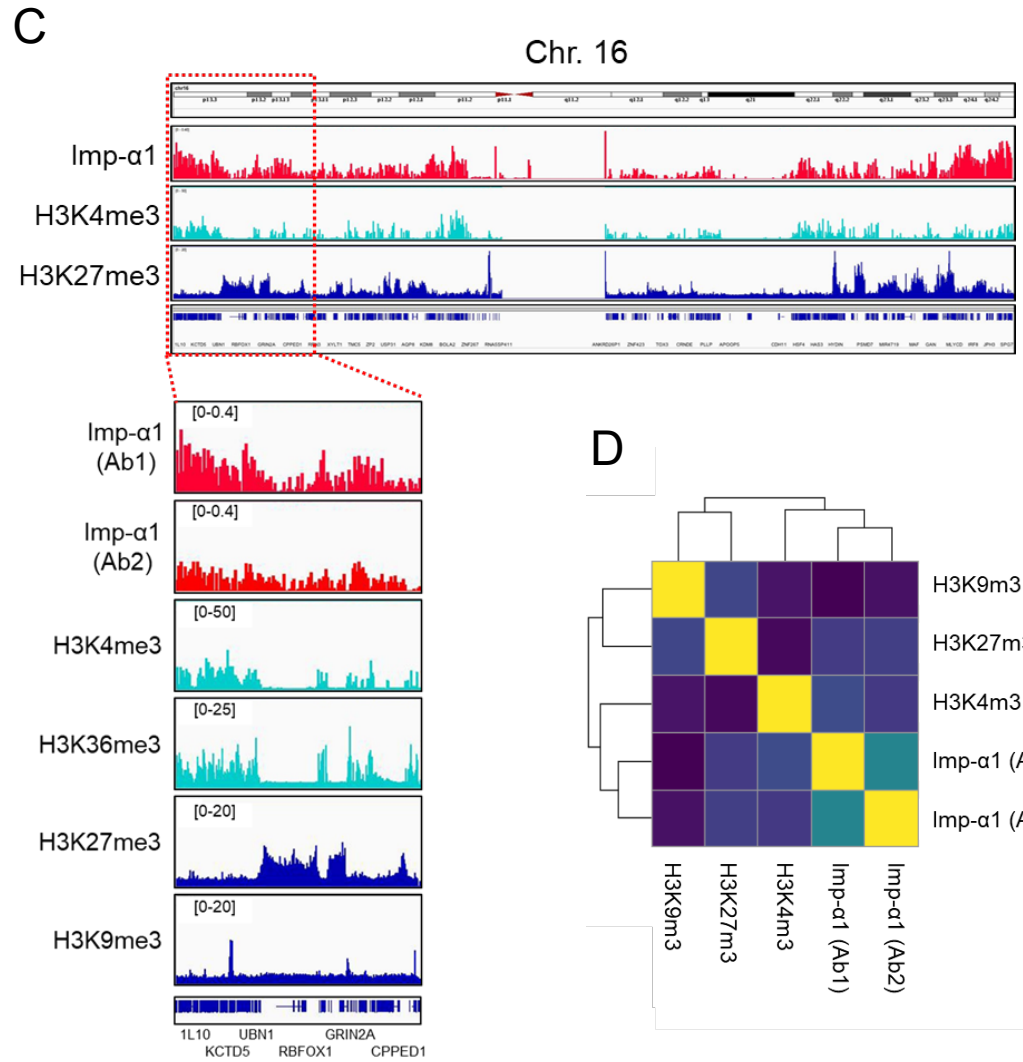
C
Chr. 16
Imp-α1
H3K4me3
H3K27me3
Imp-α1 (Ab1)
[0-0.4]
Imp-α1 (Ab2)
[0-0.4]
H3K4me3
[0-50]
H3K36me3
[0-25]
H3K27me3
[0-20]
H3K9me3
[0-20]
1L10
UBN1
GRIN2A
KCTD5
RBFOX1
CPPED1

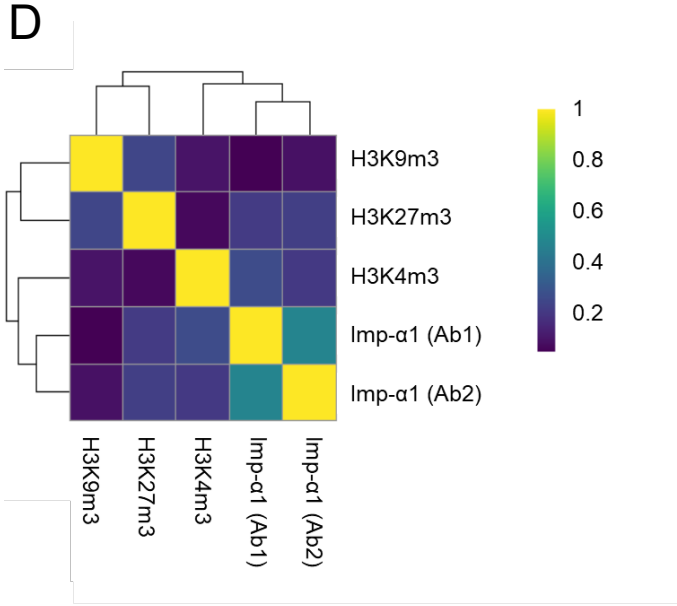
D
H3K9m3
H3K27m3
H3K4m3
Imp-α1 (Ab1)
Imp-α1 (Ab2)
1
0.8
0.6
0.4
0.2

A

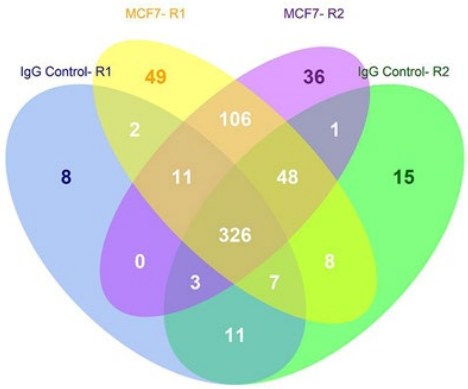
MCF7- R1
MCF7- R2
IgG Control- R1
IgG Control- R2
49
36
2
106
1
8
11
48
15
326
0
8
3
7
11

B

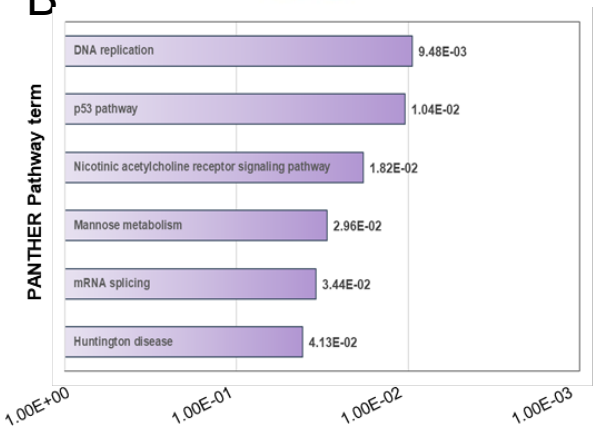
PANTHER Pathway term
DNA replication
9.48E-03
p53 pathway
1.04E-02
Nicotinic acetylcholine receptor signaling pathway
1.82E-02
Mannose metabolism
2.96E-02
mRNA splicing
3.44E-02
Huntington disease
4.13E-02
1.00E+00
1.00E-01
1.00E-02
1.00E-03

C

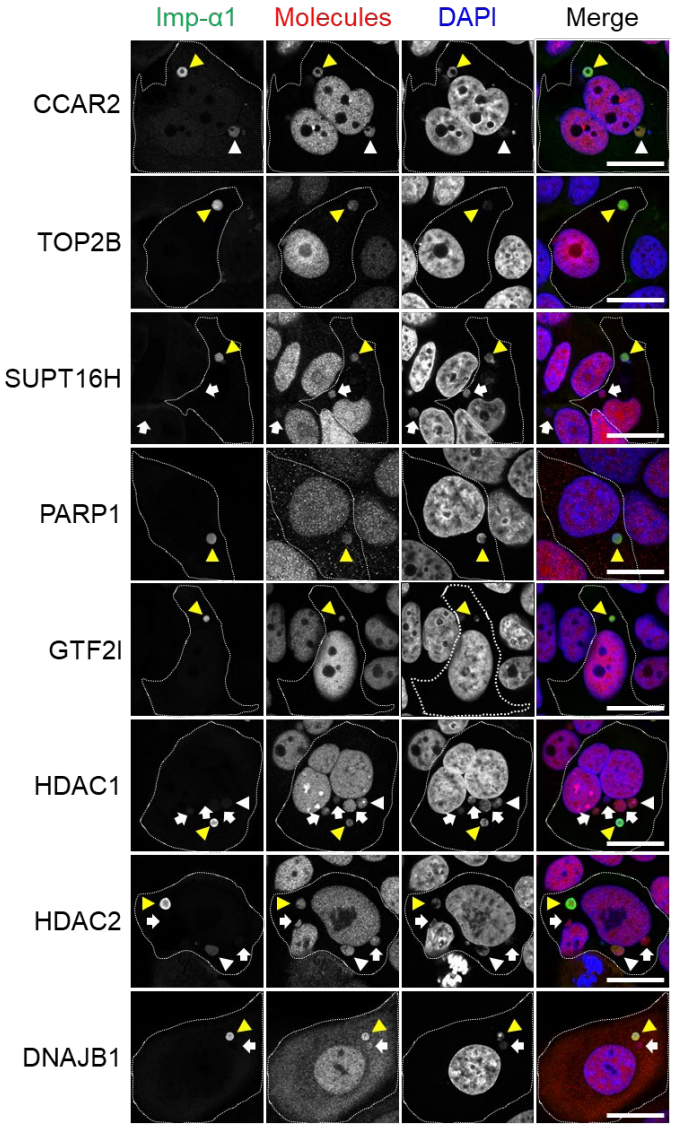
Imp-α1
Molecules
DAPI
Merge
CCAR2
TOP2B
SUPT16H
PARP1
GTF2I
HDAC1
HDAC2
DNAJB1

D

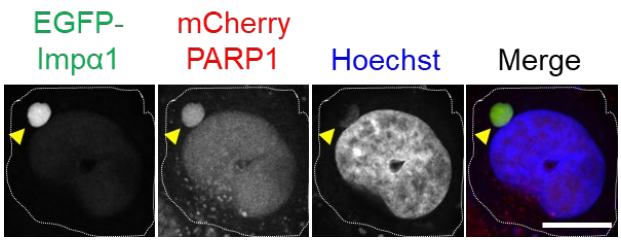
EGFP-Impα1
mCherry PARP1
Hoechst
Merge

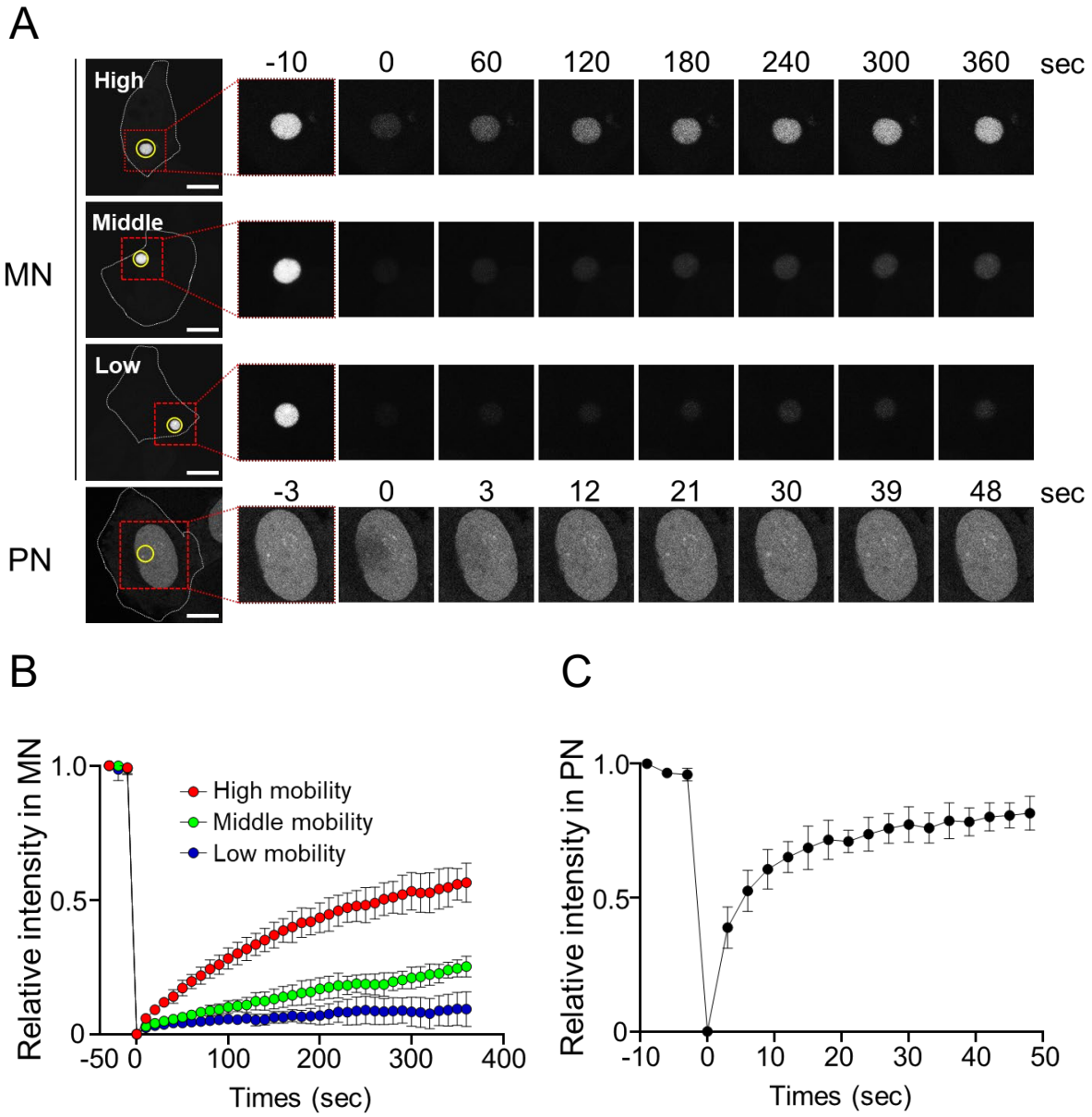
A
High
Middle
Low
MN
PN
-10
0
60
120
180
240
300
360
sec
-3
0
3
12
21
30
39
48
sec
B
Relative intensity in MN
1.0
0.5
0
-50
0
100
200
300
400
Times (sec)
High mobility
Middle mobility
Low mobility
C
Relative intensity in PN
1.0
0.5
0
-10
0
10
20
30
40
50
Times (sec)

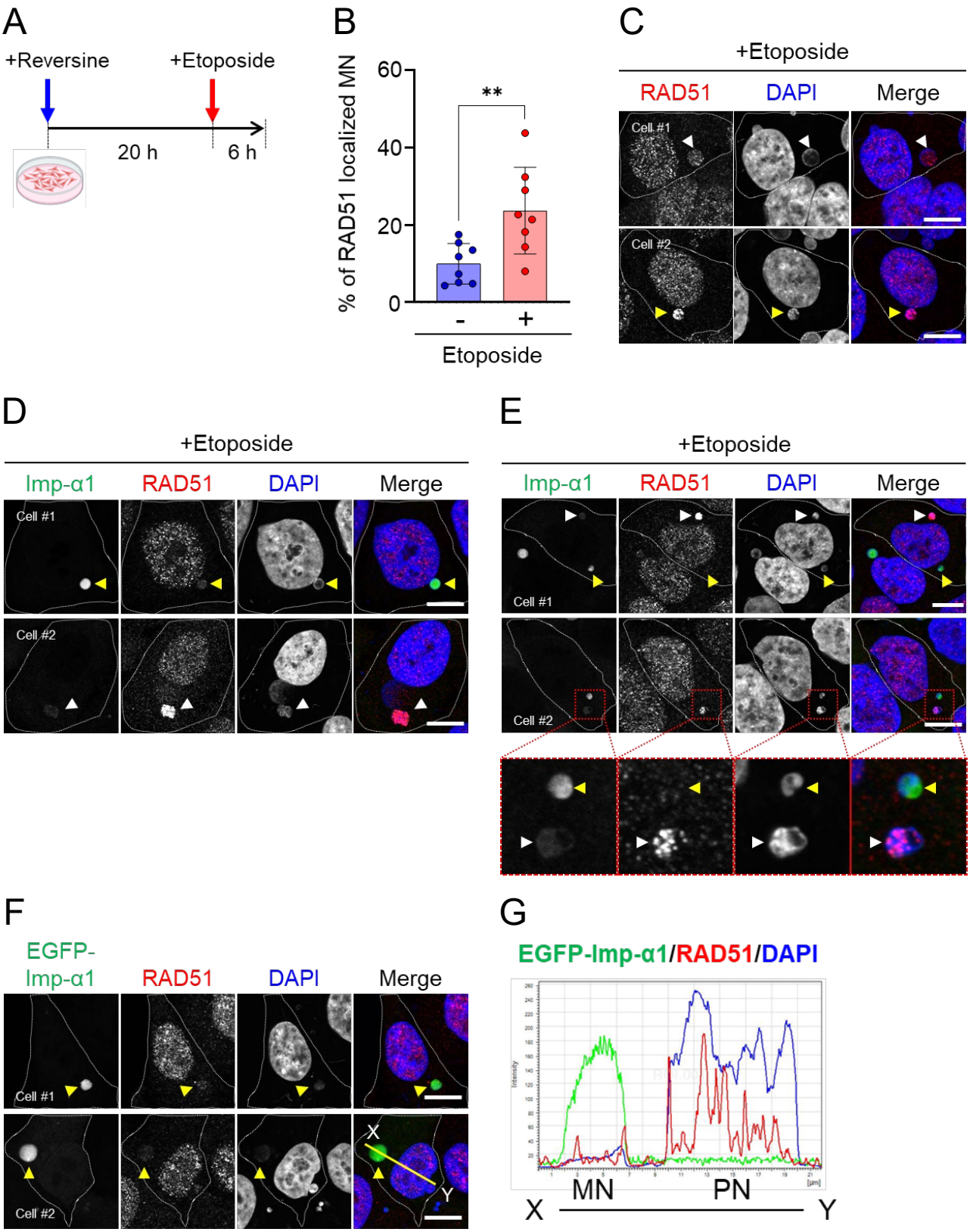
A
+Reversine
+Etoposide
20 h
6 h
B
% of RAD51 localized MN
60
40
20
0
**
-
+
Etoposide
C
+Etoposide
RAD51
DAPI
Merge
Cell #1
Cell #2
D
+Etoposide
Imp-α1
RAD51
DAPI
Merge
Cell #1
Cell #2
E
+Etoposide
Imp-α1
RAD51
DAPI
Merge
Cell #1
Cell #2
F
EGFP-Imp-α1
RAD51
DAPI
Merge
Cell #1
Cell #2
X
Y
G
EGFP-Imp-α1/RAD51/DAPI
MN
PN
X
Y
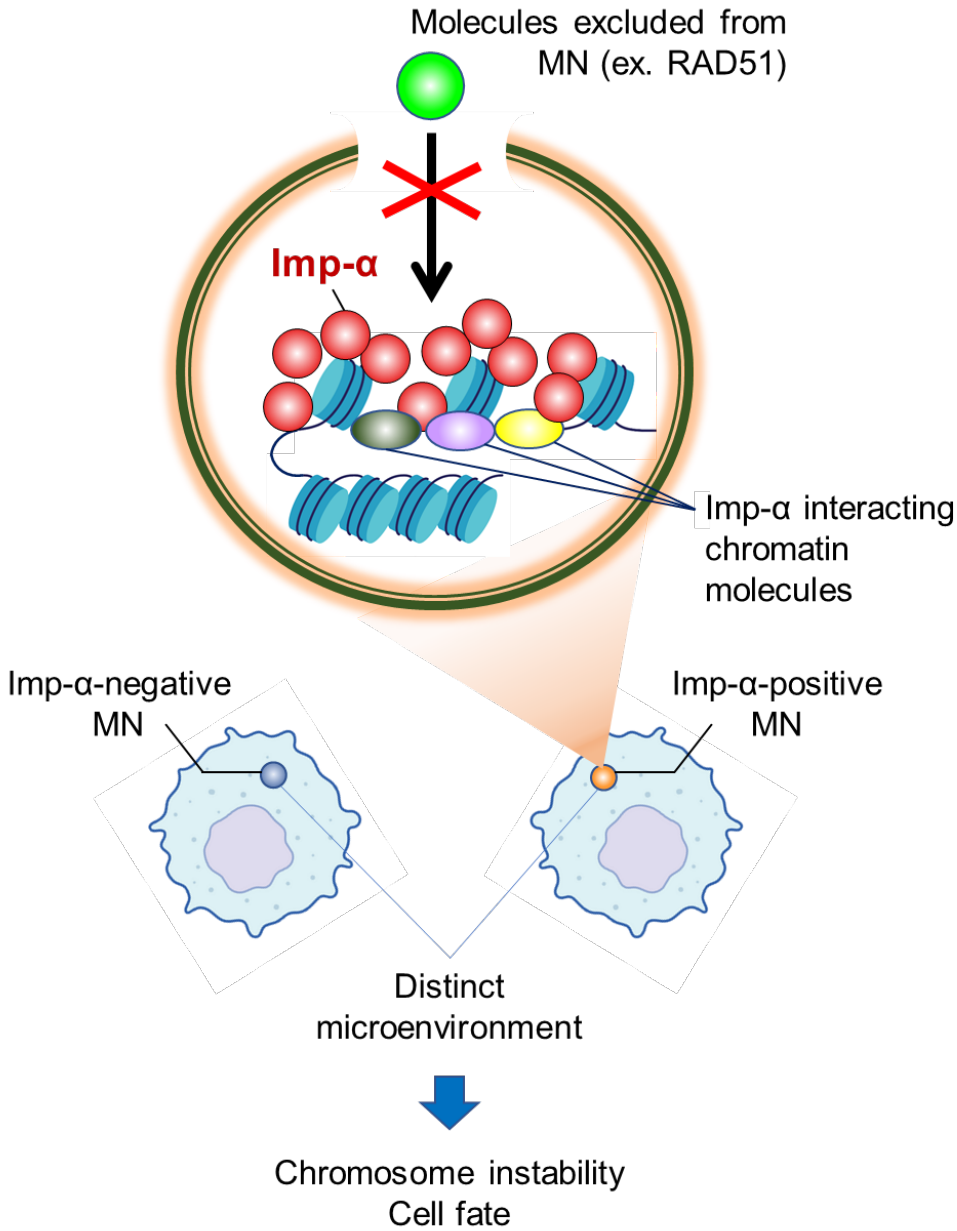
Miyamoto et al., Fig. 8